Int J Earth Sci (Geol Rundsch) (2017) 106:1469–1486
DOI 10.1007/s00531-015-1282-z

ORIGINAL PAPER

Early Paleozoic accretionary orogenesis along northern margin of Gondwana constrained by high-Mg metaigneous rocks, SW Yunnan

Xiaowan Xing[1] · Yuejun Wang[1,2] · Peter A. Cawood[3,4] · Yuzhi Zhang[1]

Received: 14 August 2015 / Accepted: 29 November 2015 / Published online: 14 December 2015
© Springer-Verlag Berlin Heidelberg 2015

Abstract SW Yunnan of China constituted part of the northern margin of Gondwana facing the proto-Tethys ocean in the early Paleozoic. However, the evolution of the region and its relationship with the accretionary orogenism have been poorly established. This paper reports a set of new zircon U–Pb age data and whole-rock major oxides, elemental and Sr–Nd isotopic data for early Paleozoic metavolcanic rocks from the previously defined Lancang Group and reveals the development of an Ordovician suprasubduction zone in SW Yunnan. Zircon U–Pb ages of 462 ± 6 and 454 ± 27 Ma for two representative samples indicate eruption of the volcanic rocks in the Late Ordovician. Geochemical data for the metavolcanic rocks together with other available data indicate a calc-alkaline affinity with high Al_2O_3 (13.04–18.77 wt%) and low TiO_2 (0.64–1.00 wt%). They have Mg-numbers ranging from 62 to 50 with SiO_2 of 53.57–69.10 wt%, compositionally corresponding to the high-Mg andesitic rocks. They display enrichments in LREEs and LILEs with significant Eu negative anomalies (δEu = 0.20–0.33), and depletions in HFSEs, similar to arc volcanic rocks. Their initial $^{87}Sr/^{86}Sr$ ratios range from 0.721356 to 0.722521 and $\varepsilon Nd(t)$ values from −7.63 to −7.62 with Nd model ages of 2.06–2.10 Ga. Integration of ages and geochemical data with available geological observations, we propose the presence of Ordovician magmatism related to proto-Tethyan evolution in SW Yunnan and the metaigneous rocks formed in an island-arc setting. They were part of a regional accretionary orogen that extended along the northern margin of Gondwana during Neoproterozoic to early Paleozoic period.

Keywords Metaigneous rocks · Lancang Group · Late Ordovician · Proto-Tethyan evolution · SW Yunnan

Introduction

Early Paleozoic igneous rocks, ranging in age from 525 to 460 Ma, exposed within the Himalayan Orogen Belt in NW India, Nepal, South Tibet and SW China (Bhanot et al. 1979; DeCelles et al. 1998, 2000, 2004; Godin et al. 2001; Xu et al. 2005; Liu et al. 2006; Gehrels et al. 2006; Cawood et al. 2007; Chen et al. 2007; Song et al. 2007; Zhang et al. 2008; Dong et al. 2009; Liu et al. 2009; Qi et al. 2010; Shi et al. 2010; Wang et al. 2011, 2012, 2013b; Li et al. 2012; Zhu et al. 2012a, b; Xing et al. 2015). In addition, Cambrian and Ordovician sequences are separated by an angular unconformity in NW India, Nepal and South Tibet (Brookfield 1993; Valdiya 1995; Le Fort et al. 1994; Hughes 2002; Liu et al. 2002; Zhou et al. 2004; Myrow et al. 2006a, b). In the early Paleozoic, these regions constituted part of the northern margin of Gondwana facing the proto-Tethys ocean. However, the detailed geological evolution of these regions during this time has poorly been established due to

✉ Yuejun Wang
wangyuejun@mail.sysu.edu.cn

1 School of Earth Science and Geological Engineering, Sun Yat-Sen University, No. 135, Xingang Xi Road, Guangzhou 510275, People's Republic of China

2 CAS Center for Excellence in Tibetan Plateau Earth Sciences, Beijing 100101, People's Republic of China

3 Department of Earth Sciences, University of St Andrews, North Street, St Andrews KY169AL, UK

4 Centre for Exploration Targeting, School of Earth Environment, University of Western Australia, 35 Stirling Highway, Crawley, WA 6009, Australia

the hinder of late Paleozoic disruption and Cenozoic tectonothermal reworking associated with Tethys closure and Himalayan orogenic formation, respectively (e.g., Dewey et al. 1988; Metcalfe 1996, 2002, 2006, 2011, 2013; Yin and Harrison 2000; Yi et al. 2011; Pan et al. 2012; Cawood et al. 2013). Two end-member tectonic models have been proposed for the early Paleozoic orogenic event involving: (a) Pan-African orogeny associated with either the breakup of an earlier supercontinent or the final assembly of Gondwana (Murphy and Nance 1991; Miller et al. 2001; Xu et al. 2005; Yang et al. 2012); and (b) Andean-type orogeny following Gondwana assembly, caused by subduction of the proto-Tethyan Ocean beneath the Indian Craton and its adjacent micro-continental blocks (Cawood et al. 2007; Zhang et al. 2008, 2012b; Dong et al. 2010; Wang et al. 2011, 2012, 2013b; Zhu et al. 2012a).

The Sanjiang (also named Nujiang-Lancangjiang-Jinshajiang in Chinese literature) area in SW Yunnan (SW China) is an important area of the eastern Tethyan tectonic belt and preserved numerous geological relicts, which is associated with the final closure of the proto-Tethys ocean (e.g., Zhang et al. 1985; Cong et al. 1993; Zhong 1998; Wang et al. 2010, 2012; Liu et al. 2009). Early Paleozoic granitic rocks, gneiss and amphibolite with age around 499–462 Ma are recently identified within the Gongshan, Tengchong-Baoshan and Shan-Thai blocks in SW Yunnan (Chen et al. 2007; Song et al. 2007; Liu et al. 2009; Li et al. 2012; Yang et al. 2012; Wang et al. 2013b). These rocks are benefit for better understanding the tectonic setting of the area and tectonic affinity of the Gongshan, Tengchong-Baoshan and Shan-Thai blocks. For example, Fang et al. (1990) suggested that there is no affinity between the Tengchong-Baoshan Block and Gondwana. However, more and more data show the Tengchong-Baoshan and Shan-Thai Blocks are the micro-segments of the Gondwana (Metcalfe 1996; Zhong 1998; Liu et al. 2009; Wang et al. 2013b; Nie et al. 2014; Xing et al. 2015). The systematic works for the associated early Paleozoic igneous are required for probing the petrogenesis and tectonic setting of SW Yunnan. In this study, we reported Laser Ablation Induction Coupled Plasma Mass Spectroscopy (LA-ICP-MS), Sensitive High-Resolution Ion Microprobe (SHRIMP II) zircon U–Pb ages and geochemical data of the metaigneous rocks in the previously defined Lancang Group to constrain the source characteristics of the magma and discuss the tectonic implication on the accretionary orogenic history of the northern margin of Gondwana.

Geological background and petrography

Southwest Yunnan is one of the important branches of eastern Tethyan tectonic belt. The Tethyan–Alpine orogenic system has a change in direction from the Himalayan segment (WNW-trending) to the Southeast Asian segment (northerly trending) in SW Yunnan (Fig. 1a; Hutchison 1989; Metcalfe 1996, 2002, 2013; Zhang et al. 2008, 2012b; Wang et al. 2013b). The area includes Simao/Indochina, Baoshan/Shan-Thai and Tengchong blocks (Fig. 1a) which were separated by the Changning–Menglian and Longling–Ruili faults, respectively. The Simao/Indochina Block consists of a Proterozoic metamorphosed succession of pyroclastic rocks and carbonates (Zhong 1998), unconformably overlain by a Paleozoic package of carbonate and siliciclastic rocks with typical Cathaysia flora and fauna (Yunnan BGMR 1990; Zhong 1998; Feng 2002). The Baoshan, Tengchong and Shan-Thai blocks are components of the Sibumasu continental fragment and display stratigraphic and paleontological affinities to Gondwana continent (Fig. 1a, b; Fan and Zhang 1994; Metcalfe 1996, 2002; Zhong 1998; Feng 2002; Fontaine 2002; Wang et al. 2013b).

The Lancang Group is a set of metamorphic volcano-sedimentary cycles, mainly exposed in Baoshan and Shan-Thai Blocks. The stratigraphic package includes pre-Mesozoic high-grade metamorphic rocks and Mesozoic–Cenozoic sedimentary and igneous rocks (Yunnan BGMR 1990; Zhong 1998; Wang et al. 2013b). Previous study considered this group consisting of four formations, which are in ascending order the Mengjingshan, Manlai, Huimin and Nankenghe Formations (Fig. 1c; Yunan BGMR 1979). The Mengjingshan Formation with thickness of over 300 m is mainly composed of light quartzite, granulite, sericite schist and sericite quartz schist in its upper part. The typical flysch sedimentary rocks indicate that the stratum is a production of high-speed accumulation with the crust subsidence intensely. The Manlai Formation consists of subdivide cycles from coarse to fine grains. The lower cycle is about 1400 m thick, and the upper cycle is nearly 1300 m thick; they predominantly consist of feldspathic quartz sandstone, gray sericite microcrystalline schist, sericite quartz schist, mica schist and metavolcanic rocks (Wei et al. 1984; Wu et al. 1984; Yunnan BGMR 1990; Shen et al. 2008). The Huimin Formation, 2500 m thick, comprises metamorphic basalt, andesite, andesitic tuff, rhyolitic tuff, and a few Fe-siliceous slate inbedding chlorite phyllite, sericite phyllite, chlorite schist, siderite layer and marble lens. The strata of Nankenghe Formation are mainly low metamorphic rocks, the structure and construction are less destroyed. The Nankenghe Formation is characterized by silica quartz sandstone, sericite quartz sandstone and microcrystalline schist in about 1000 m thick (Wei et al. 1984; Wu et al. 1984; Yang et al. 2012; Nie et al. 2014).

The Huimin Formation mainly exposed in Huimin and Manlai areas. Our study focuses on the Huimin Formation in both areas, and sampling locations are displayed in

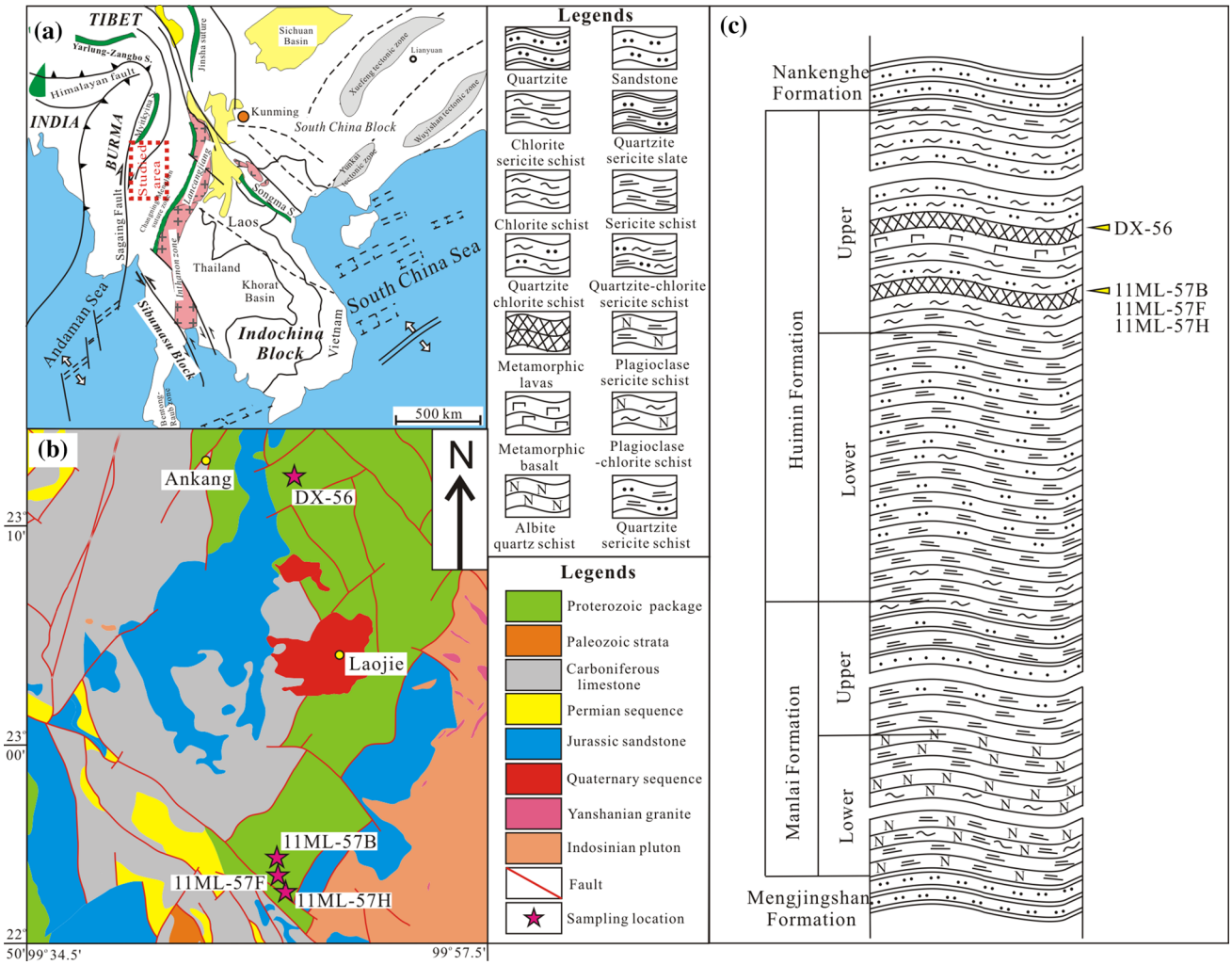

Fig. 1 **a** Tectonic outline of Southeast Asian, **b** simplified geological map revised from 1:200,000 geological map of Cangyuan in SW Yunnan and **c** Stratigraphic column of the Lancang Group (revised from 1:200,000 geological map of Jinghong, Yunnan)

Fig. 1b, c. The represent samples (11ML-57B, -57F and -57H and DX-56) are andesites metamorphosed to lower-greenschist facies. They are dark-green in color with a schistose fabric and composed of feldspar, albite and chlorite along with the accessory mineral phases of titanite, apatite, zircon and Fe–Ti oxides. The major oxides and trace elemental data of the samples for the volcanic rocks in the Huimin Formation in the current study have been documented in Shen et al. (2008) and Nie et al. (2014).

Analytical methods

Zircon U–Pb LA-ICP-MS method

Zircons were separated using conventional heavy liquid and magnetic techniques and then purified by handpicking under a binocular microscope. After mounting in epoxy, polishing and coating of grains with carbon, the samples were photographed in transmitted and reflected light. The internal textures of zircons were examined using cathodoluminescence (CL) imaging prior to U–Pb isotopic analyses at the Institute of Geology and Geophysics (IGG), Chinese Academy of Sciences (CAS). U–Pb isotope analysis was conducted by Nu Plasma HR MC-ICPMS (Nu Instruments) with ArF-193 nm laser-ablation system (Resolution M-50) in the University of Hong Kong (11ML-57H). The instrumental settings and detailed analytical procedures have been described in Wu et al. (2006), Geng et al. (2014) and Gong et al. (2014). We used standards GJ-1 and 91500 to determine the elemental fractionation during sputter ionization. Off-line selection and integration of background and signals, time-drift correction and quantitative calibration were conducted by ICPMSDataCal (Liu et al. 2010). Zircon U–Pb age concordia and weighted average plots were

Table 1 LA-ICP-MS and SHRIMP zircon U–Pb dating results of the previously defined Lancang Group metavolcanic rocks

Samples	Th/U	Isotopic ratio						Apparent age (Ma)					
		$^{207}Pb/^{206}Pb$	±%	$^{207}Pb/^{235}U$	±%	$^{206}Pb/^{238}U$	±%	$^{207}Pb/^{206}Pb$	±1σ	$^{207}Pb/^{235}U$	±1σ	$^{206}Pb/^{238}U$	±1σ
11ML-57 (LA-ICP-MS zircon U–Pb dating)													
11ML-57-01	0.55	0.0541	0.30	0.5598	3.10	0.0748	0.24	376	119	451	20	465	15
11ML-57-02	0.54	0.0597	0.32	0.6018	3.23	0.0728	0.24	591	112	478	20	453	14
11ML-57-03	0.69	0.0594	0.32	0.6170	3.26	0.0750	0.25	583	115	488	20	466	15
11ML-57-04	0.77	0.0563	0.27	0.5836	2.75	0.0741	0.24	465	99	467	18	461	14
11ML-57-05	0.58	0.0606	0.31	0.6252	3.21	0.0736	0.24	633	110	493	20	458	15
11ML-57-07	0.72	0.0540	0.31	0.5646	3.22	0.0752	0.25	372	128	455	21	468	15
11ML-57-08	0.59	0.0553	0.25	0.5679	2.59	0.0739	0.24	433	104	457	17	459	14
11ML-57-09	0.73	0.0521	0.25	0.5394	2.60	0.0744	0.24	300	109	438	17	462	14
11ML-57-10	0.74	0.0576	0.27	0.5888	2.80	0.0736	0.24	517	104	470	18	458	14
11ML-57-11	0.55	0.0515	0.26	0.5364	2.75	0.0748	0.24	265	117	436	18	465	15
11ML-57-12	0.50	0.0536	0.29	0.5514	3.02	0.0739	0.25	354	119	446	20	460	15
11ML-57-13	0.67	0.0509	0.25	0.5149	2.57	0.0727	0.23	235	112	422	17	452	6
11ML-57-14	0.75	0.0539	0.28	0.5531	2.83	0.0741	0.25	365	119	447	19	461	15
11ML-57-15	0.52	0.0520	0.30	0.5406	3.05	0.0747	0.25	287	131	439	20	464	15
11ML-57-16	0.60	0.0544	0.27	0.5718	2.86	0.0752	0.24	387	82	459	18	467	15
11ML-57-17	0.61	0.0523	0.29	0.5380	2.96	0.0741	0.24	298	126	437	20	461	15
11ML-57-18	0.65	0.0531	0.27	0.5541	2.78	0.0743	0.24	345	113	448	18	462	14
11ML-57-19	0.71	0.0515	0.29	0.5406	2.95	0.0756	0.25	261	128	439	19	470	15
11ML-57-20	0.57	0.0517	0.29	0.5361	3.05	0.0746	0.25	333	97	436	20	464	15
11ML-57-21	0.59	0.0540	0.30	0.5553	3.08	0.0742	0.25	369	131	448	20	462	15
11ML-57-22	0.83	0.0543	0.27	0.5599	2.74	0.0740	0.24	383	83	451	18	460	14
11ML-57-23	0.60	0.0543	0.31	0.5580	3.22	0.0741	0.24	389	126	450	21	461	15
11ML-57-24	0.50	0.0523	0.34	0.5380	3.31	0.0752	0.25	302	148	437	22	468	15
11ML-57-25	0.71	0.0531	0.30	0.5503	3.15	0.0741	0.24	332	130	445	21	461	15
DX-56 (SHRIMP zircon U–Pb dating)													
DX56-2	0.57	0.1591	0.46	7.6162	1.81	0.3472	1.75	2446	8	1809	32	1921	29
DX56-3	1.32	0.0667	3.39	1.1904	4.06	0.1295	2.23	827	71	784	17	785	16
DX56-4	1.03	0.0685	2.15	1.5462	2.85	0.1636	1.88	885	44	981	18	977	17
DX56-5	0.47	0.0555	3.06	0.5536	3.53	0.0724	1.77	430	68	451	8	451	8
DX56-6	1.53	0.0649	2.29	1.0756	2.87	0.1202	1.74	771	48	731	12	732	12
DX56-7	1.25	0.1623	1.50	10.440	2.69	0.4666	2.24	2480	25	2464	65	2469	46
DX56-8	0.40	0.0668	3.06	1.4670	3.66	0.1592	2.01	832	64	957	19	953	18
DX56-9	1.37	0.1046	1.66	4.5891	2.61	0.3182	2.02	1708	30	1791	36	1781	31
DX56-10	0.81	0.1626	0.77	10.977	2.48	0.4896	2.36	2483	13	2610	77	2569	50
DX56-11	0.57	0.0640	0.76	1.1453	1.87	0.1299	1.71	741	16	788	13	787	13
DX56-12	0.73	0.0552	3.50	0.5323	3.99	0.0700	1.91	420	78	436	8	436	8
DX56-13	1.26	0.0743	2.26	1.7207	2.94	0.1680	1.89	1050	46	999	18	1001	17
DX56-14	0.72	0.0722	0.97	1.7372	2.03	0.1746	1.78	991	20	1039	18	1037	17
DX56-15	0.59	0.0557	2.62	0.5630	3.26	0.0733	1.94	440	58	456	9	456	9
DX56-16	2.17	0.0557	3.69	0.5993	4.15	0.0780	1.91	442	82	485	9	484	9
DX56-17	1.52	0.0707	5.18	1.5575	5.59	0.1597	2.09	950	106	955	19	955	19
DX56-18	0.87	0.0976	0.67	3.8674	1.85	0.2873	1.73	1579	13	1634	28	1628	25
DX56-19	0.33	0.0613	1.59	0.9419	2.33	0.1114	1.70	651	34	681	11	681	11
DX56-20	0.93	0.0532	3.11	0.5413	3.57	0.0738	1.75	337	70	461	8	459	8
DX56-21	0.04	0.0655	0.73	1.2700	1.84	0.1407	1.69	790	15	850	14	848	13
DX56-22	0.49	0.0583	2.48	0.6086	3.07	0.0757	1.81	540	54	470	8	471	8
DX56-23	0.46	0.0500	6.18	0.4802	6.46	0.0696	1.90	197	143	437	8	434	8

made by Isoplot (Ludwig 2003). The analytical results are listed in Table 1.

Zircon U–Pb SHRIMP method

The treatment processes of zircons before instrument tests are the same as we have introduced above. The zircons were analyzed for Pb–Th–U isotopes using the SHRIMP II ion microprobe at the Curtin University (DX-56), Australia. The instrumental conditions and data acquisition procedures are similar to those described by Williams and Claesson (1987) and Williams (1998). The SHRIMP runs in a primary ion beam of ca. 1.6–3.0 nA, 10 kV of O^{2-}. Spots size range between 20 and 30 μm and each analysis site is rastered over 120 μm for 2 min to reduce any common Pb on the surface or contamination from the gold coating. The instrumental settings and detailed analytical procedures have been described in Williams (1998), Black et al. (2003) and Zi et al. (2012a, b). To maintain precision, one TEMORA analysis was performed after every three or four spots on the sample zircons during data collection. The common lead correction was applied using the measured ^{204}Pb value (Compston et al. 1984). Errors for individual analyses are at 1σ level, unless otherwise stated. Uncertainties are quoted with 95 % confidence limits. Sites for dating were selected on the basis of CL and microscope images. Software SQUID 1.0 and Isoplot (Ludwig 2003) were used for data processing. The analytical results are listed in Table 1.

Geochemistry method

Samples were crushed and powdered to less than 200 mesh for whole-rock geochemical analysis at Langfang Integrity Geological Ltd., Hebei Province. Major oxides were determined by a XRF-100e spectrometry in the Guangzhou Institute of Geochemistry (GIG), CAS. Analytical error is usually <1 %, and detection limit is <0.05 % for most major elements. For trace elements, the rock powders were first digested by HF + HNO_3 in Teflon bombs and then analyzed on IsoProbe MC-ICPMS in the GIG, CAS. Analytical precision is generally better than 5 % for most elements. Detailed sample-processing digesting procedure and analytical precision and accuracy for major elements and trace elements are described by Ma et al. (2014) and Liang et al. (2003), respectively. The analytical results for major and trace elements are shown in Table 2.

Sr and Nd isotopic ratios were measured by MCICP-MS at the GIG, CAS. The analytical procedures are the same as reported by Wei et al. (2002). The total procedure blanks are in the range of 200–500 pg for Sr and <50 pg for Nd. The mass fractionation corrections for Sr and Nd isotopic ratios were based on $^{86}Sr/^{88}Sr = 0.1194$ and $^{146}Nd/^{144}Nd = 0.7219$, respectively. The measured $^{87}Sr/^{86}Sr$ ratio of (NIST) SRM 987 standard and the $^{143}Nd/^{144}Nd$ ratio of the La Jolla standard are 0.710265 ± 12 (2σ) and 0.511862 ± 10 (2σ), respectively. $^{143}Nd/^{144}Nd$ and $^{147}Sm/^{144}Nd$ ratios of CHUR at the present time used for calculating εNd value are 0.512638 and 0.1967, respectively. $^{87}Rb/^{86}Sr$ and $^{147}Sm/^{144}Nd$ ratios were calculated using the Rb, Sr, Sm and Nd abundances measured by ICP-MS. The measured and age-corrected $^{87}Sr/^{86}Sr$ and $\varepsilon Nd(t)$ are listed in Table 2.

Results

Zircon U–Pb geochronology

Zircon U–Pb dating was undertaken on samples 11ML-57H and DX-56 with the former analyzed by LA-ICP-MS and the latter by the SHRIMP method. The data are shown in Table 1 and Fig. 2.

The zircon grains from 11ML-57H are mostly euhedral and short-columnar in morphology, transparent and colorless, and generally small in size (60–100 μm, 1:1-2:1 for length/width; Fig. 2a). Th/U ratios of twenty-four grains are in the range of 0.46–0.83 (Table 1). These analyses cluster around 460 Ma (Fig. 2a), yielding a weighted mean $^{206}Pb/^{238}U$ age of 462 ± 6 Ma with MSWD = 0.1 ($n = 24$; Fig. 2b). The CL images reveal oscillatory zonation with low to variable luminescence (Fig. 2a), together with high Th/U ratios, indicating an igneous origin (Hoskin and Black 2000; Wu and Zheng 2004). The age of 462 ± 6 Ma is interpreted as the eruption age of the sample.

Twenty-two spots on 22 grains were analyzed from sample DX-56. Zircons are mostly euhedral and short-columnar with well-developed oscillatory zoning, typical of a magmatic origin (Fig. 2c). Two major age peaks are present at around 456 and 794 Ma (Fig. 2c). Three spots give older ages around 2480 Ma. Only one spot has a Th/U ratio value of less than 0.1 (DX-56-21), whereas the other twenty-one spots have U and Th concentration of 25–703 ppm and 28–632 ppm, respectively, with the Th/U ratios ranging from 0.33 to 2.17 (Table 1). Thus, these ages with more than 790 Ma can be interpreted as inherited grains. Seven of twenty-two spots yield a weighted mean $^{206}Pb/^{238}U$ age of 454 ± 27 Ma with MSWD = 0.2 ($n = 7$; Fig. 2d), interpreted as the formation age of the sample.

Geochemical characteristics

Our geochemical data, together with the published data for the Huimin metavolcanic rocks (Shen et al. 2008; Nie et al. 2014), are used to constrain their petrogenesis and tectonic settings of Ordovician magmatic rocks along the

Table 2 Major oxides (wt%), trace element (ppm) and Sr–Nd isotopic analyses for the Ordovician metavolcanic rocks in SW Yunnan

Sample	Manlai			Huimin*						Manlai*	
	11ML-57B	11ML-57F	11ML-57H	D008	D009	D010	D011	H4	H5	H9	H10
SiO_2	62.74	62.94	55.42	63.88	65.01	53.88	53.57	63.35	59.63	54.96	69.10
TiO_2	0.66	0.64	0.87	0.66	0.77	0.72	0.72	1.00	0.97	0.92	0.90
Al_2O_3	16.34	16.18	17.04	14.58	17.40	13.72	13.68	16.85	15.32	18.77	13.04
FeOt	6.72	6.34	8.58	6.30	7.31	11.32	11.66	8.20	9.02	13.24	8.61
MnO	0.10	0.10	0.14	0.08	0.06	0.16	0.16	0.14	0.16	0.25	0.12
MgO	3.60	3.21	5.91	3.74	4.16	7.30	7.58	4.37	4.32	9.12	3.76
CaO	4.88	5.03	6.06	6.37	0.51	10.04	9.92	0.52	7.74	0.19	1.03
Na_2O	3.28	3.32	3.40	1.03	0.35	1.30	1.13	4.52	0.88	1.05	0.49
K_2O	1.55	2.14	2.45	3.21	4.27	1.33	1.35	0.78	1.62	1.35	2.25
P_2O_5	0.11	0.11	0.12	0.15	0.16	0.23	0.22	0.26	0.34	0.14	0.70
LOI	2.19	1.94	2.45	7.92	4.38	3.30	3.36	3.87	3.51	6.81	3.90
Total	99.79	99.81	99.63	99.29	98.81	98.88	98.74	99.66	99.20	99.23	99.36
Mg-number	55	54	62	58	57	60	60	55	53	62	50
Sc	14.40	15.40	19.20	16.85	22.31	37.28	37.39	41.80	47.40	51.50	36.20
V	102	99	159	89	117	222	223	308	340	380	303
Cr	53	41	113	161	198	547	551	197	357	1236	971
Co	14.6	15.2	22.9	35.9	46.6	84.4	91.5	42.2	48.1	1070	72.4
Ni	34.3	30.0	70.7	63.3	75.4	173	181	46.7	73.2	597.	337
Rb	68	87	97	110	164	65	66	41	100	87	134
Sr	266	307	288	94	10	536	539	58	436	55	70
Y	23.00	21.70	25.10	25.25	27.06	21.47	21.92	43.70	37.50	15.20	27.10
Zr	95	94	95	141	162	91	90	233	180	170	137
Nb	6.90	6.76	6.05	10.45	12.46	5.36	5.38	13.00	11.20	8.27	7.62
Ba	384	603	521	594	883	660	804	279	593	1124	2075
La	26.90	20.90	20.30	21.51	22.89	15.26	15.62	54.50	32.00	14.30	23.30
Ce	51.30	43.90	41.70	46.61	51.22	31.80	32.66	101.00	63.90	28.70	38.60
Pr	6.05	5.15	5.00	5.21	5.80	3.94	3.98	13.50	7.78	3.55	6.44
Nd	23.30	20.40	20.30	20.80	23.07	16.26	16.64	54.10	32.20	14.20	27.70
Sm	5.10	4.54	4.99	4.42	4.99	3.62	3.79	10.10	6.97	3.16	6.11
Eu	1.15	1.06	1.28	0.94	0.98	0.98	1.01	2.12	1.64	0.99	1.91
Gd	4.92	4.41	4.86	4.35	4.61	3.62	3.79	8.71	6.69	2.85	5.45
Tb	0.83	0.77	0.82	0.73	0.77	0.59	0.62	1.43	1.13	0.44	0.89
Dy	5.12	4.72	5.06	4.46	4.70	3.68	3.92	7.84	6.50	2.65	5.10
Ho	0.91	0.86	0.97	0.90	0.98	0.75	0.78	1.60	1.31	0.57	1.00
Er	2.60	2.43	2.75	2.60	2.92	2.25	2.42	4.56	3.79	1.83	2.74
Tm	0.40	0.37	0.41	0.40	0.45	0.36	0.38	0.67	0.54	0.28	0.38
Yb	2.45	2.21	2.50	2.52	2.76	2.35	2.43	4.40	3.61	2.47	2.49
Lu	0.40	0.37	0.42	0.36	0.40	0.34	0.34	0.67	0.51	0.41	0.39
Hf	3.21	3.28	3.02	4.02	4.80	2.52	2.48	6.79	4.97	4.94	3.91
Ta	0.65	0.62	0.55	0.88	1.09	0.43	0.43	0.95	0.75	0.49	0.37
Th	12.4	10.4	8.51	11.77	14.46	6.60	6.61	21.50	7.26	7.26	7.59
Eu*	0.23	0.24	0.26	0.21	0.20	0.27	0.27	0.23	0.24	0.33	0.33
ΣREE	170.69	148.08	148.55	157.75	173.96	116.82	119.82	338.14	219.05	104.29	161.47
$(La/Yb)_N$	7.88	6.79	5.83	6.12	5.94	4.66	4.61	8.89	6.36	4.15	6.72
$(Nb/La)_N$	0.25	0.31	0.29	0.47	0.52	0.34	0.33	0.23	0.34	0.56	0.32
$^{143}Nd/^{144}Nd$	0.512054	0.512060									
2σ	7	6									

Table 2 continued

Sample	Manlai			Huimin*						Manlai*	
	11ML-57B	11ML-57F	11ML-57H	D008	D009	D010	D011	H4	H5	H9	H10
$^{87}Sr/^{86}Sr$	0.721356	0.722521									
2σ	14	11									
$^{87}Sr/^{86}Sr(i)$	0.716492	0.717149									
$\varepsilon Nd(t)$	−7.63	−7.62									
T_{DM} (Ga)	2.06	2.10									

Data for Huimin* and Manlai* are from Shen et al. (2008) and Nie et al. (2014)

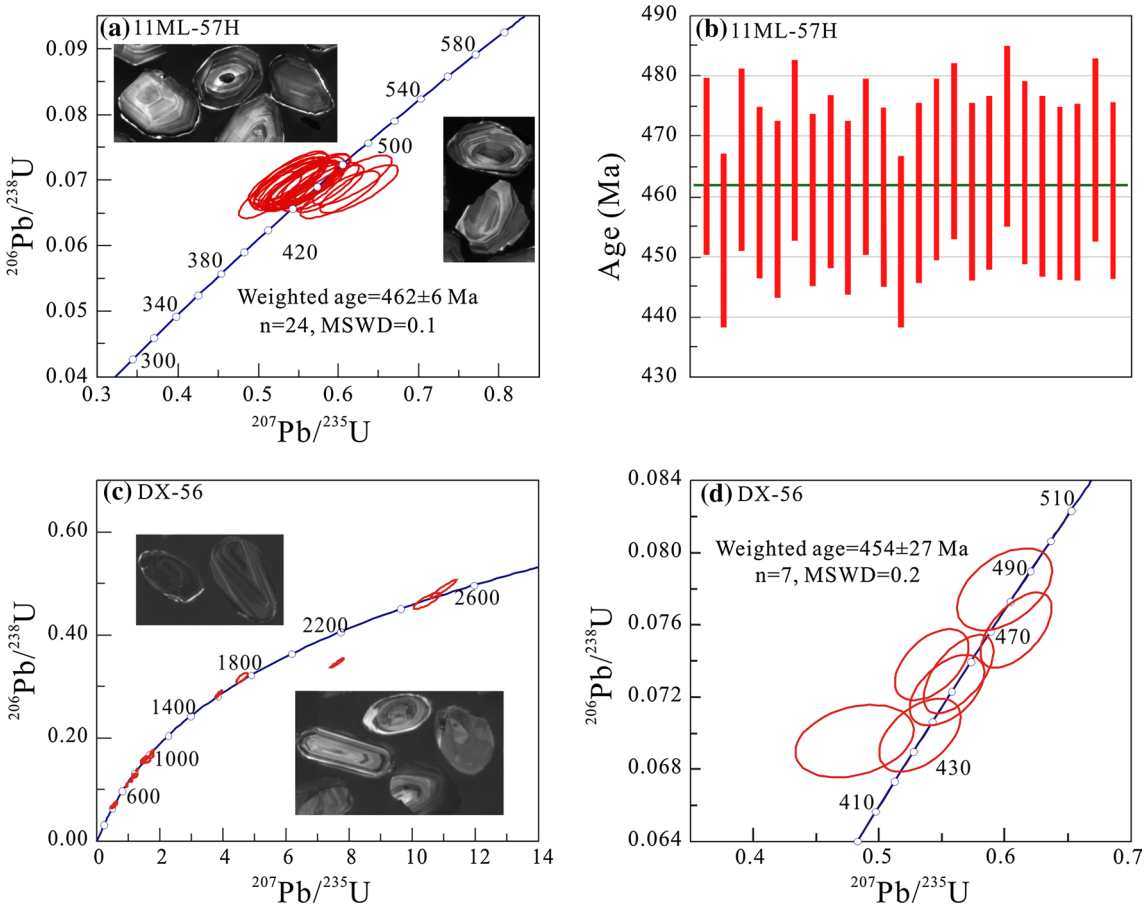

Fig. 2 Zircon U–Pb age concordia and weighted average plots for 11ML-57H (**a**, **b**) and DX-56 (**c**, **d**), respectively. The sampling locations are shown in Fig. 1b, c

proto-Tethyan margin of Gondwana continent. Loss on ignition (LOI) values for the samples range from 1.94 to 7.92 wt% (Table 2), suggesting that these rocks might have undergone some degree of low-temperature alteration (Rolland et al. 2002). In the plots of Zr and incompatible elements (Fig. 3a–f), these samples show linear correlation, suggestive of the insignificant mobile during the low-temperature alteration. Thus, only concentrations and ratios of the immobile elements (e.g., HFSEs and REEs) are used.

The metaigneous rocks contain 53.57–69.10 wt% SiO_2 and 0.11–0.70 wt% P_2O_5 and are characterized by low TiO_2 (0.64–1.00 wt%) and high Al_2O_3 contents (13.04–18.77 wt%). The samples plot in the fields of basaltic andesite and andesitic rocks on the Nb/Y–Zr/TiO_2 × 10^{-4} plot (Fig. 4a; Winchester and Floyd 1977). Their MgO contents range from 3.21 to 9.12 % with Mg-numbers of 50–62, higher than those of normal arc volcanic rocks (e.g., NE Japan arc) at comparable SiO_2 (Table 2; Fig. 4b). Thus

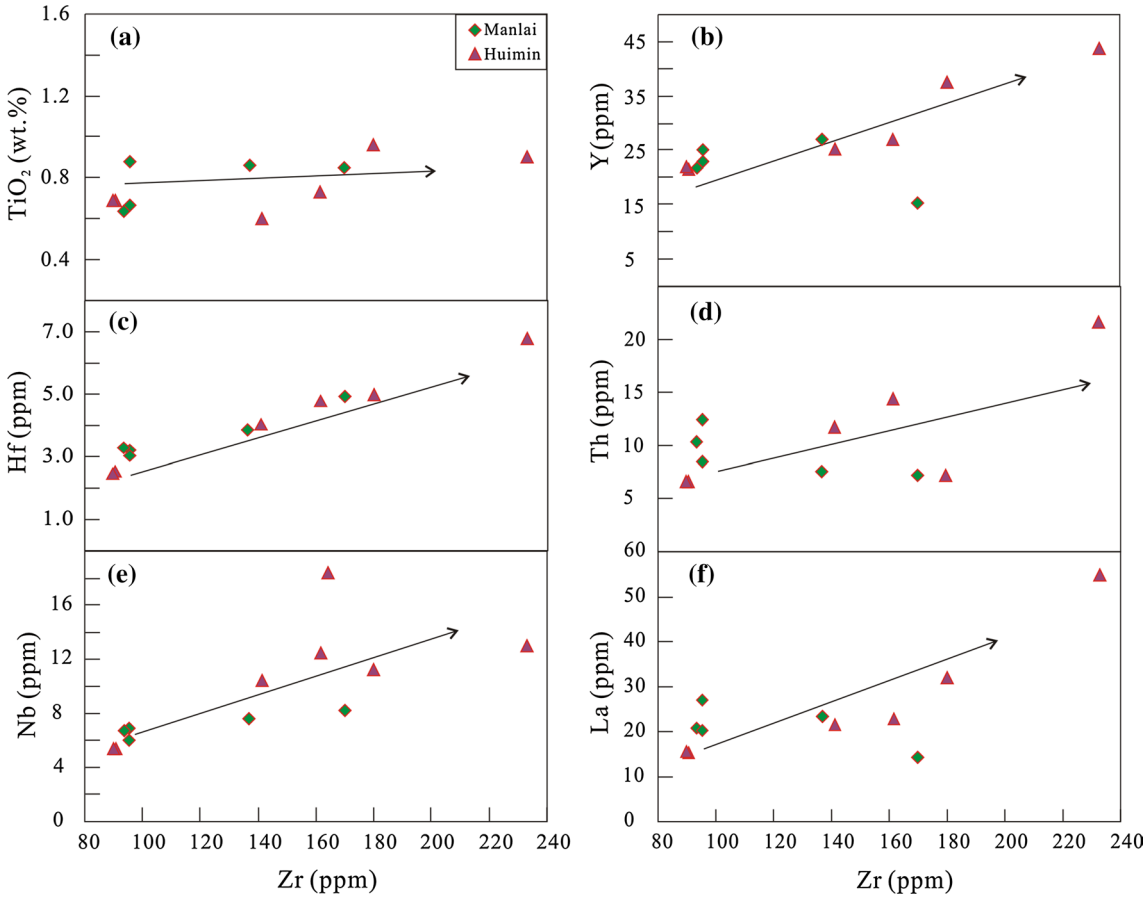

Fig. 3 Zr (ppm) versus **a** TiO_2 (wt%), **b** Y (ppm), **c** Hf (ppm), **d** Th (ppm), **e** Nb (ppm) and **f** La (ppm) for the Ordovician metavolcanic rocks in the previously defined Lancang Group (SW Yunnan)

these samples can be classified as high-Mg rocks according to the classification scheme of Kelemen (1995), as shown in Fig. 4b. They display geochemical characteristics similar to those of the Archean calc-alkaline sanukitoids of the Superior, Finland, Dharwar and Amazonian cratons (Fig. 4c; Shirey and Hanson 1984, 1986; Stern et al. 1989; Smithies and Champion 2000; Moyen et al. 2003; Halla 2005; Tatsumi 2008; Oliveira et al. 2009). These metaigneous samples have similar MgO and Na_2O contents to those of the sanukitoid high-Mg andesite in the Japanese volcanic belt and low-silica adakite at comparable SiO_2 (Fig. 4c; Tatsumi 2001, 2006, 2008; Moyen et al. 2003). On the Sr/Y–Y diagram (Fig. 4d; Kamei et al. 2004), they are generally plotted in the range of the sanukitoid high-magnesium andesite. Al_2O_3, FeOt, CaO and MgO generally show negative correlations with SiO_2, but little correlations exist between SiO_2 and TiO_2 and P_2O_5 (Fig. 5a–f).

The samples show similar chondrite-normalized REE patterns (Fig. 6a) and have moderately fractionated light rare-earth elements (LREEs) relative to heavy rare-earth elements (HREEs), with $(La/Yb)_N$ = 4.15–8.89 (Table 2). All the samples show negative Eu anomalies with Eu* = 0.20–0.33. On the primitive mantle-normalized incompatible element spider diagram (Fig. 6b), these samples are characterized by subparallel spiky patterns with enrichment in LILEs and depletion in HFSEs with significantly negative Nb–Ta anomalies [$(Nb/La)_N$ = 0.23–0.56] but insignificantly negative Zr–Hf anomalies [$(Hf/Sm)_N$ = 0.87–2.25]. Three samples from Manlai area show weakly negative Sr anomalies, contrary to typical adakite with pronounced positive Sr anomalies. Such patterns, irrespective of SiO_2 content, are similar to those of the typical arc volcanic rocks.

Two samples (11ML-57B and 11ML-57H) were analyzed for Sr–Nd isotopic compositions. The measured $^{87}Sr/^{86}Sr$ ratios are 0.721356 and 0.722521, respectively. The $^{143}Nd/^{144}Nd$ values are 0.512054 and 0.512060, respectively. The initial Sr isotopic ratios back-calculated to 460 Ma are 0.7165 and 0.7171, and $\varepsilon Nd(t)$ values are −7.63 and −7.62. The corresponding T_{DM} values are 2.06 and 2.10 Ga for 11ML-57B and 11ML-57F (Table 2), respectively.

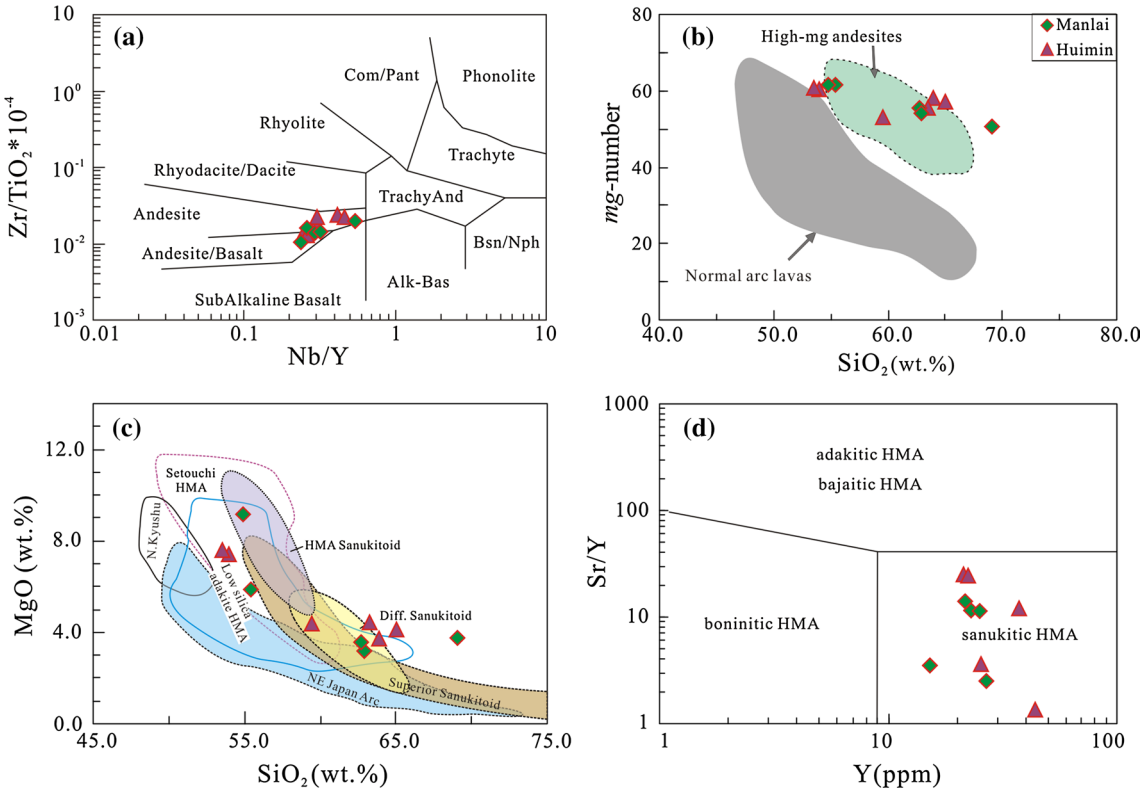

Fig. 4 **a** Classification diagram of **a** Nb/Y versus $Zr/TiO_2 \times 10^{-4}$, **b** SiO_2 (wt%) versus Mg-number, **c** SiO_2 (wt%) versus MgO (wt%) and **d** Y (ppm) versus Sr/Y for the Ordovician (454–460 Ma) volcanic rocks. The ranges for different rocks including normal arc lavas, Archean sanukitoids, Setouchi HMA are from Stern et al. (1989), Middlemost (1994), Kelemen (1995), Smithies and Champion (2000), Tatsumi (2001), Halla (2005), and Oliveira et al. (2009)

Discussion

Formation age of the Lancang metavolcanic sequence

The Lancang Group is composed of a metamorphic volcanic-sedimentary package, predominantly constituted by quartzite-schist, sandstone-volcanics, volcanics-schist and sandstone-schist, respectively. Previous estimations about the age of the package range from Mesoproterozoic to Paleozoic. Yunnan BGMR (1982) had assumed it to be the Mesoproterozoic sequence. These rocks were mapped as the Neoproterozoic sequence in the geological map of Jinghong and Menghai (Yunnan BGMR 1990). Zhong (1998) ascribed it as part of the Yangtze basement on the basis of a whole-rock Sm–Nd isochron age of 1982 ± 41 Ma from the Huimin Formation of the Lancang Group. Zhai et al. (1990) concluded that the Huimin volcanic rocks erupted during early Paleozoic based on a whole-rock Rb–Sr isochron age of 519 Ma. Shen et al. (2008) stated that the Huimin Formation was pre-Devonian sequence.

Our samples from the previously defined Lancang Group yielded weighted mean $^{206}Pb/^{238}U$ zircon ages of 462 ± 6 ($n = 24$) and 454 ± 27 Ma ($n = 7$), respectively. The CL structures of these grains have typical oscillatory zonation, and Th/U ratios range from 0.33 to 2.17 (except spot DX-56-21 with Th/U value of 0.04). Thus these ages can be interpreted as the eruption age of the metavolcanic rocks. Nie et al. (2014) recently obtained a U–Pb zircon age of 456 ± 7 Ma for the andesitic sample of the Huimin Formation. Thus, the previously defined Lancang Group, at least Huimin volcanic sequence, is most likely formed during the Ordovician period.

Origin of the Ordovician high-Mg andesitic rocks

All analyzed samples show little or no correlation between the LOI and Zr, La and Nb/La and Th/La, suggesting insignificant modification of elemental contents during low-temperature alteration. SiO_2 correlates negatively with CaO and CaO/Al_2O_3 (Fig. 5b, g), indicative of fractionation of clinopyroxene and hornblende during magma evolution. This is also evidenced by the negative correlation between SiO_2 and MgO, FeOt and Al_2O_3 (Fig. 5a, c, d). Apatite and Fe–Ti oxides fractionation should be insignificant since TiO_2 and P_2O_5 contents are relatively constant irrespective of Zr (Fig. 3a) or SiO_2 (Fig. 5e, f). Plagioclase fractionation

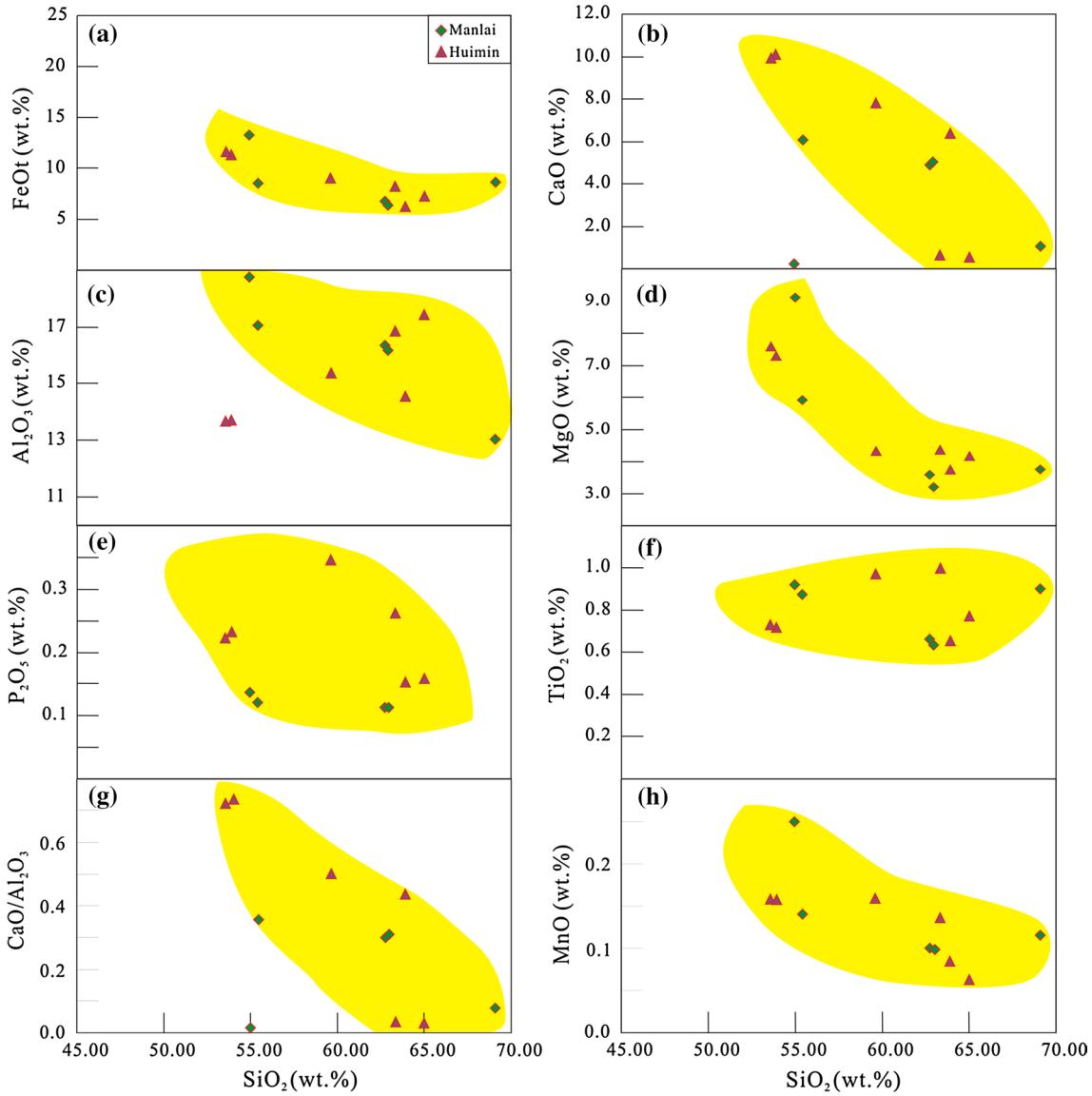

Fig. 5 SiO_2 (wt%) versus **a** FeOt (wt%), **b** CaO (wt%), **c** Al_2O_3 (wt%), **d** MgO (wt%), **e** P_2O_5 (wt%), **f** TiO_2 (wt%), **g** CaO/Al_2O_3 and **h** MnO (wt%) for the Ordovician metavolcanic rocks in the previously defined Lancang Group (SW Yunnan)

is marked by negative correlations of CaO and Al_2O_3 with SiO_2 (Fig. 5b, c) and significantly negative Eu anomalies (Fig. 6).

The samples have negative $\varepsilon Nd(t)$ values (−7.63 and −7.62) and $^{147}Sm/^{144}Nd$ ratios of 0.132459–0.134479. $T_{DM}(Nd)$ ages of 2.06–2.10 Ga are much older than their formation age (~460 Ma). They exhibit similar initial Sr–Nd isotopic compositions to the Ordovician granitic rocks in SW Yunnan, the Greater Himalayan Crystalline Complex, and Lhasa metarhyolite, and also fall into the fields of the Greater Himalayan Crystalline Complex metasedimentary rocks and Ordovician S-type granites in the Lachlan Fold Belt (Fig. 7; Healy et al. 2004; Wang et al. 2007). The $\varepsilon Nd(t)$ values are significantly lower than the synchronous Mandi and Shao La mafic rocks in Greater Himalayan Crystalline Complex and Lhasa metabasites (Miller et al. 2001; Chen et al. 2007; Liu et al. 2009; Wang et al. 2011, 2012; Zhu et al. 2011, 2012a, b; Wang et al. 2013b).

Three petrogenetic models have been proposed for the high-Mg andesitic rocks involving the partial melting of (1) eclogitic crust, (2) a young and hot slab, or (3) metasomatized source modified by the subduction-related components (Baker and Stolper 1994; Kelemen 1995; Yogodzinski et al. 1995; Hirose 1997; McCarron and Smellie 1998; Shimoda et al. 1998; Kawabata and Shuto 2005; Wang et al. 2006, 2009; Hoang et al. 2009; Zhang et al.

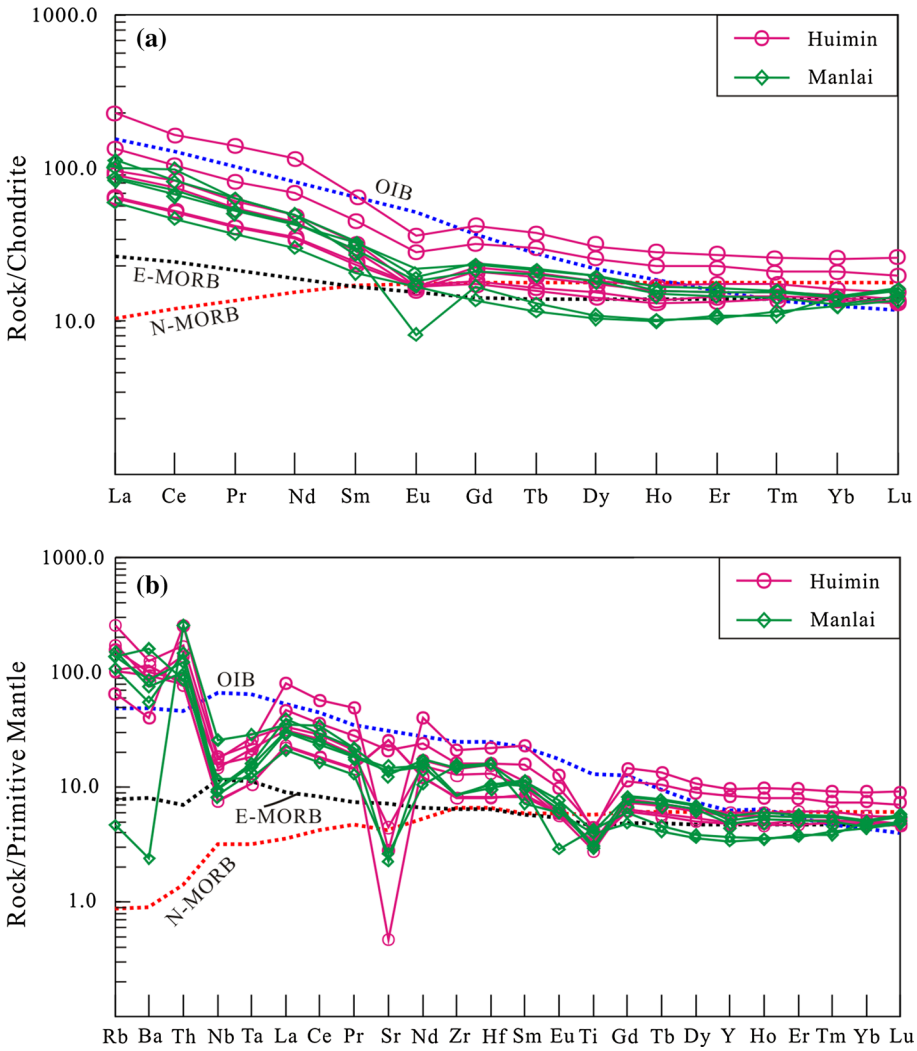

Fig. 6 **a** Chondrite-normalized REE patterns and **b** primitive mantle-normalized incompatible element for the Ordovician metavolcanic rocks. Normalized values for chondrite and primitive mantle are from Sun and McDonough (1989)

2012a; Honarmand et al. 2015). We firstly argue that cases (1) and (2) are not applicable to the Lancang high-Mg metavolcanic rocks based on the following observations. Our samples have relatively high Mg-numbers (50–62), Al_2O_3 (13.04–18.77 wt%) and low TiO_2 (0.64–1.00 wt%) contents, enrichment in LILEs and depletion in HFSEs (Fig. 6b) with high LILE/HFSE ratios. The partial melting of a granulite or eclogite crust, containing minor rutile, generally produces magma with low Mg-number, high Al_2O_3 (>17 %) and TiO_2 contents (Rapp et al. 1991, 1999; Sen and Dunn 1994). Thus, the Lancang metavolcanic rocks are unlikely to be derived from the melting of an eclogitic crust. Our high-Mg metavolcanic andesitic samples have weakly negative Eu, Ba and Sr anomalies, indicative of the absence of plagioclase in the source. In addition, the samples exhibit insignificant Ce anomalies, relatively high $^{87}Sr/^{86}Sr(t)$ ratios and negative $\varepsilon Nd(t)$ values, against the possible model for derivation of a hot and young subducted slab for these rocks (Defant and Drummond 1990; Kelemen et al. 1993).

Melt extraction or slab- and sediment-derived metasomatism at exceptionally low pressures can form a high modal orthopyroxene source and lead to relatively high SiO_2 contents in the rocks (Kushiro 1990; Gallagher and Hawkesworth 1992; Chalot-Prat and Boullier 1997). As a result, the arc-like elemental signatures (e.g., high LREE and LILE contents, high La/Nb, Ba/Th and Ba/La ratios and negative Nb–Ta–Ti anomalies) and the "crust-like" Sr–Nd isotopic compositions of the analyzed samples are likely attributed to a source modified by recycled sediment- or slab-derived components (Rapp et al. 1991, 1999; Evans and Hanson 1997; Sajona et al. 2000; Smithies and Champion 2000; Prouteau et al. 2001; Moyen et al. 2003; Smithies et al. 2003, 2007; Kamei 2004; Oliveira et al. 2009). High-Mg andesites that originate from a slab-metasomatized source (e.g., western Aleutians) generally exhibit high Sr contents and La/Yb ratios and depleted Sr–Nd isotopic system. However, our samples show insignificant Sr anomalies and EMII-like isotopic composition. Their Sr/La ratios gently increase

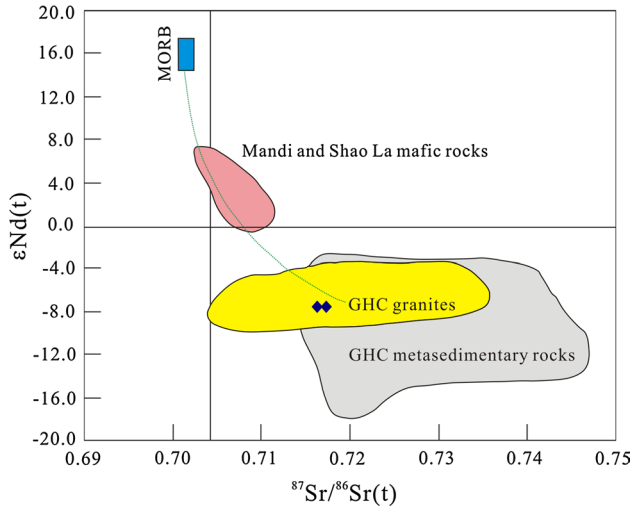

Fig. 7 Initial Sr–Nd isotopic composition. The Sr–Nd isotopic data for Mandi and Shao La mafic rocks, along with the granite and metasedimentary rocks of the Greater Himalayan Complex (GHC), are from Parrish and Hodges (1996), Robinson et al. (2001), Imayama and Arita (2008), Miller et al. (2001), Visonà et al. (2010), Zhu et al. (2012a) and Wang et al. (2011, 2012)

with decreasing La/Yb ratios and the Th/Yb ratios increase with increasing Ba/La ratios (not shown). The Th/Yb ratios of Lancang high-Mg metavolcanic rocks range from 2.01 to 5.23, obviously higher than N-MORB (0.04; Sun and McDonough 1989) and E-MORB (0.25; Sun and McDonough 1989), having been ascribed to the addition of subducted sediments (Davidson 1987; Xu et al. 2014). As shown in the Fig. 8a, b, samples plot along the trend related to fluid-related/increasing hydrous metasomatism rather than melt-related enrichment. Such geochemical signatures appear to be consistent with the source involvement of subducted sediment rather than a slab-derived component.

Tectonic implications

Available data show that the Sanjiang area in SW Yunnan is an important component of the orogenic zone associated with the final closure of the proto-Tethys ocean basin (Zhang et al. 1985; Cong et al. 1993; Zhong 1998). Evidence for early Paleozoic tectonothermal activity is widespread along the northern margin of East Gondwana from NW India to SW Yunnan involving an unconformity separating Ordovician from older strata, along with Cambrian–Ordovician magmatic activity, metamorphism and deformation (Cawood et al. 2007; Wang et al. 2013b). Widespread development of Cambrian and Ordovician volcanic rocks including acid and basic tuffs, basalts, andesites and felsic volcanic rocks in the western Tethyan Himalaya resembles to those from volcanic arc systems (Garzanti et al. 1986; Brookfield 1993; Valdiya 1995).

The Mandi mafic rocks in High Himalayan Crystalline of NW India formed at 496 ± 14 Ma and show geochemical affinity to a convergent margin setting (Miller et al. 2001). At Shenzha in the Central Lhasa Block, Ji et al. (2009) and Zhu et al. (2012a) identified the late Cambrian (~492 Ma) bimodal volcanic rocks related to the active continental margin, which are underlain by the lower Ordovician basal conglomerate (Ji et al. 2009; Li et al. 2010). SHRIMP zircon U–Pb ages for cumulate gabbro along the Longmucuo-Shuanghu suture zone range from 467 ± 4 to 432 ± 7 Ma (Li et al. 2008; Wang et al. 2008; Zhai et al. 2010). Yang et al. (2012) reported the late Cambrian (499.2 ± 2.1 Ma) mafic lavas with geochemical affinities to arc volcanic rocks in the Gongyanghe Group, which are unconformably overlain by lower Ordovician basal conglomerate in the Baoshan Block of SW Yunnan. Wang et al. (2013a) obtained zircon U–Pb age of 473.0 ± 3.8 and 444.0 ± 4.0 Ma for cumulate gabbro with geochemical affinity to back-arc basin setting at Nantinghe

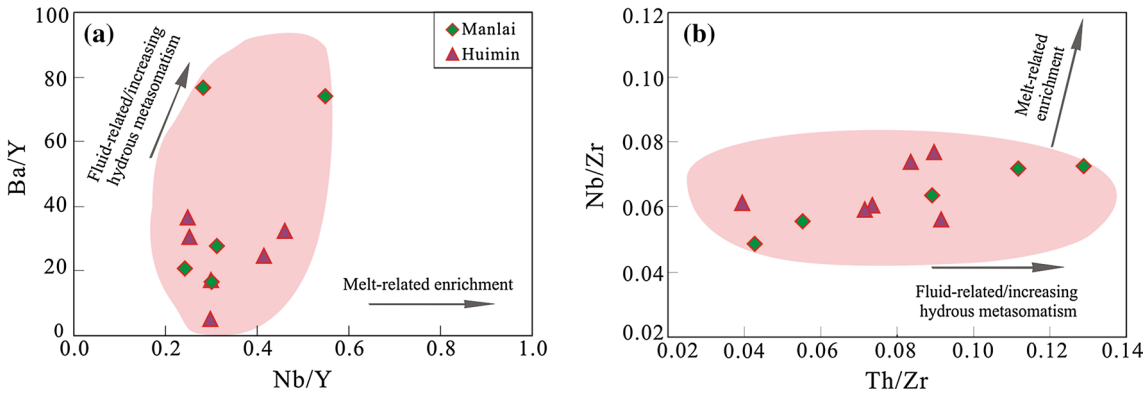

Fig. 8 **a** Nb/Y versus Ba/Y and **b** Th/Zr versus Nb/Zr for the Ordovician metavolcanic rocks showing an input of the subducted fluid-related metasomatism

in the Baoshan Block of SW Yunnan. Meanwhile, Wang et al. (2013a) obtained LA-ICPMS zircon U–Pb age of 443.6 ± 4.0 and 439.0 ± 2.4 Ma for cumulate gabbro and gabbro in the Tongchangjie ophiolitic mélange along the Changning-Menglian tectonic belt, respectively. In addition, molybdenite samples from the dacite-hosted massive sulfide deposit at Dapingzhang of the southern Lancangjiang zone, which is interpreted as a product of back-arc volcanic setting, yield the zircon U–Pb age of 429 ± 2 Ma and Re–Os isotopic ages of 429 ± 6 and 442 ± 6 Ma (Yang et al. 2008; Li et al. 2010). Medium–basic to medium–acidic island-arc volcanic rocks were separated from the Precambrian Jitang Formation and re-defined as the Lower Paleozoic Youxi Formation in the central and northern Lancangjiang zones. Our metavolcanic samples from the previously defined Lancang Group in SW Yunnan formed in the Late Ordovician around 460 Ma and are classified as high-Mg andesitic rocks. They exhibit arc-like geochemical signatures (e.g., low TiO_2, Ni, Cr and higher Al_2O_3 contents, and a marked enrichment in LILEs and LREEs and a depletion in HFSEs; Bailey 1981; Peate et al. 1997) and negative $\varepsilon Nd(t)$ values, suggestive of subduction-related metasomatic enrichment, interpreted as the derivation of the metasomatic source with the input of subducted sediment. On tectonic discrimination diagrams (Fig. 9a–c), they plot in a suprasubduction setting. In addition, the peraluminous granites in the Tengchong, Baoshan and Shan-Thai Blocks in SW Yunnan, which were generated in the active continental margin setting related to accretionary orogenesis, have the zircon U–Pb ages of 498–460 Ma (Wang et al. 2013b and reference therein). All of these observations, along with the widespread development of early Paleozoic volcanic rocks in the Tethyan Himalaya and Sanjiang areas (e.g., Brookfield 1993; Garzanti et al. 1986; Valdiya 1995), suggest an evolution of the proto-Tethyan arc-basin system during early Paleozoic in South Tibet and Sanjiang areas.

Ordovician basal conglomerate unconformably overlies the Cambrian-lower Ordovician Group in the Baoshan and Tengchong Blocks (Wang 2000), suggestive of a regional early Paleozoic orogenesis. Wang et al. (2013b) proposed the development of an early Paleozoic orogenesis from NW India to at least Namche Barwa. More importantly, the reconstruction of northeastern Gondwana at Late Ordovician indicates that the Tethyan Himalaya and associated East and Southeast Asian micro-continents (e.g., Baoshan, Tengchong, Shan-Thai, Pan-Cathaysia and Indochina) were located paleographically on the proto-Tethyan margin of East Gondwana (Fig. 10a, b; Cawood et al. 2007, 2013; Wang et al. 2010; Zhu et al. 2012a, b). Although the exact

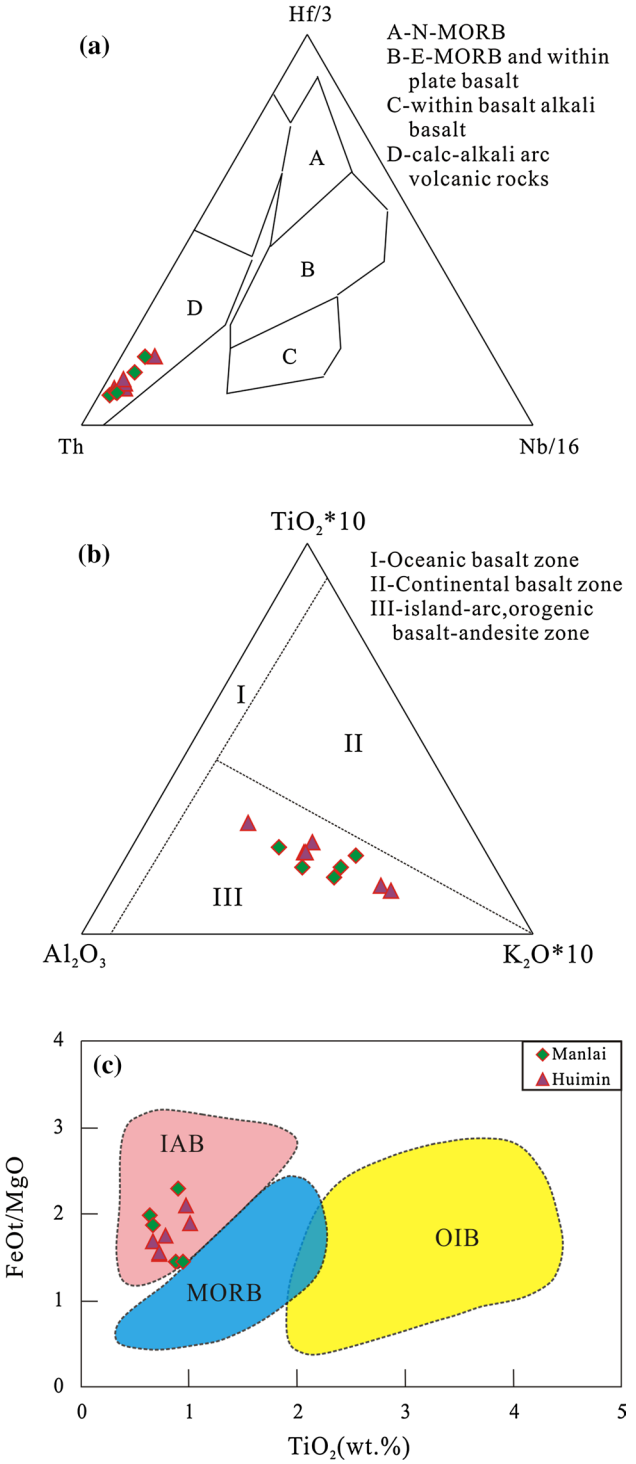

Fig. 9 **a** Th–Hf–Nb diagram (e.g., Wood 1980), **b** ATK diagram (e.g., Zhao 1989) and **c** TiO_2 (wt%)-FeOt/MgO diagram (e.g., Glassley 1974; IAB: island-arc basalt; MORB: oceanic ridge basalt; OIB: oceanic island basalt) of the Ordovician metavolcanic rocks in SW Yunnan

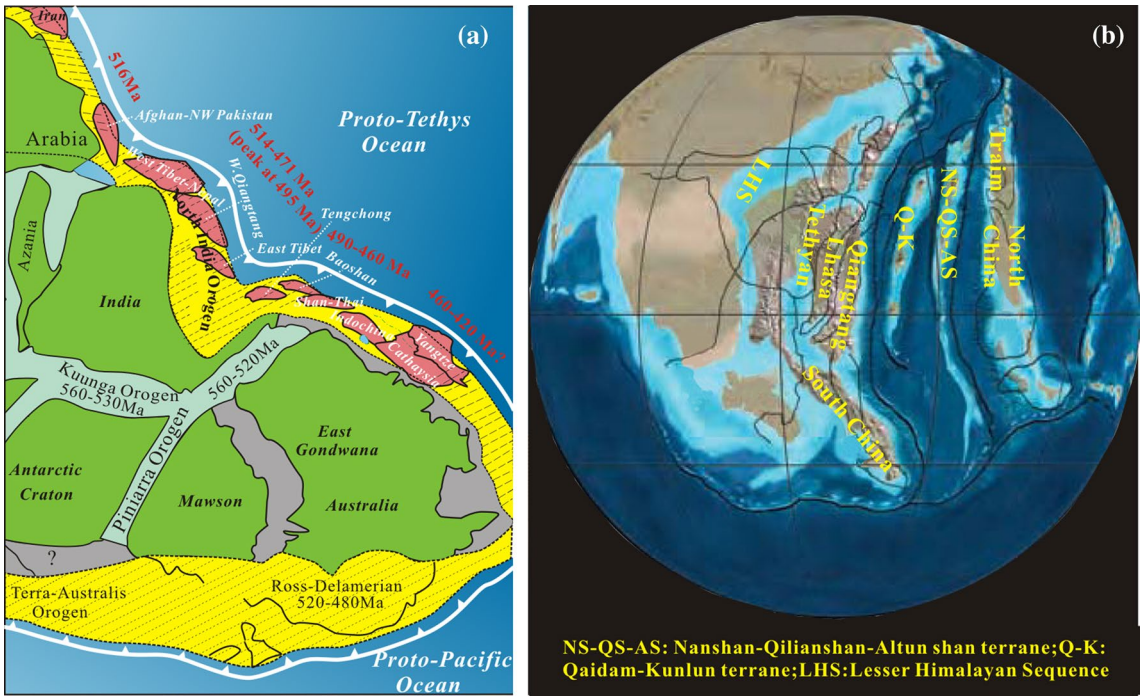

Fig. 10 **a** Tectonic reconstruction map of the India–Australia proto-Tethyan margin showing paleographical locations of the micro-continents during Ordovician (revised after Wang et al. 2010, 2013b) and **b** global paleogeographic map for the Ordovician (after Gehrels et al. 2011)

paleogeographic location of the Simao block along the East Gondwana margin is still unknown, it must be nearby or be part of the Pan-Cathaysia or Indochina blocks on basis of their paleobiological and paleoclimate affinity. Thus, these high-Mg rocks in the previously defined Lancang Group, together with synchronous mafic and granitic rocks, can be interpreted as the product of subduction of the proto-Tethyan ocean along the north margin of East Gondwana at the early Paleozoic (Chen et al. 2007; Liu et al. 2009; Zhang et al. 2008, 2012b; Wang et al. 2011, 2012, 2013b; Zhu et al. 2012a, b; Xing et al. 2015). The synthesis of our data and available regional observations suggest that these igneous rocks have been generated in a Late Ordovician island-arc setting related to subduction of the proto-Tethyan Ocean facing the Pan-Cathaysia continent. These Ordovician volcanic rocks in SW Yunnan might be the product of a regional accretionary orogen that extended along the northern margin of Gondwana during the Neoproterozoic to early Paleozoic.

Conclusions

1. The Huimin metavolcanic rocks in Manlai area of the previously defined Lancang Group of SW Yunnan give zircon U–Pb age of 462 and 454 Ma, indicative of Late Ordovician origin.
2. The volcanic rocks have Mg-numbers ranging from 62 to 50 with SiO_2 of 53.57–69.10 wt%, compositionally corresponding to the high-Mg andesitic rocks. They show relatively high Al_2O_3 and low TiO_2, with enrichments in LREE and LILEs and depletions in HFSEs, and have Eu and Nb–Ta negative anomalies. They have negative $\varepsilon Nd(t)$ (−7.62 and −7.63) and Paleoproterozoic model ages (T_{DM} of 2.10–2.06 Ga), similar to arc-like volcanic rocks.
3. These igneous rocks were derived from a mantle wedge source with involvement of subducted sediment in an Ordovician island-arc setting in response to subduction of the proto-Tethyan Ocean facing the Pan-Cathaysia.

Acknowledgments This study was supported by China Natural Science Foundation (41190073 and 41372198), National Basic Research Program of China (2014CB440901), Natural Environment Research Council (Grant NE/J021822/1) and the Fundamental Research Fund for the Central Universities to SYSU. We are grateful to Wolf-Christian Dullo, Yunpeng Dong and another anonymous reviewer for their critical and constructive reviews and comments on this paper. We would like to thank T.-P. Peng, J.-W. Zi, and L.-Y. Ma for their help during fieldwork and dating analyses.

References

Bailey JC (1981) Geochemical criteria for a refined tectonic discrimination of orogenic andesites. Chem Geol 32:139–154

Baker MB, Stolper EM (1994) Determining the composition of high-pressure mantle melts using diamond aggregates. Geochim Cosmochim Acta 58:2811–2827

Bhanot VB, Bhandari AK, Singh VP, Kansal AK (1979) Geochronological and geological studies on a granite of Higher Himalaya, northeast of Manikaran, Himachal Pradesh. J Geol Soc India 20:90–94

Black LP, Kamo SL, Allen CM, Aleinikoff JN, Davis DW, Korsch RJ, Foudoulis C (2003) TEMORA 1: a new zircon standard for Phanerozoic U–Pb geochronology. Chem Geol 200:155–170

Brookfield ME (1993) The Himalayan passive margin from Precambrian to Cretaceous times. Sed Geol 84:1–35

Cawood PA, Nemchin AA, Strachan R, Prave T, Krabbendam M (2007) Sedimentary basin and detrital zircon record along East Laurentia and Baltica during assembly and breakup of Rodinia. J Geol Soc 164:257–275

Cawood PA, Wang YJ, Xu YJ, Zhao GC (2013) Locating South China in Rodinia and Gondwana: a fragment of greater India lithosphere? Geology 41(8):903–906

Chalot-Prat F, Boullier AM (1997) Metasomatism in the subcontinental mantle beneath the Eastern Carpathians (Romania): new evidence from trace element geochemistry. Contrib Miner Petrol 129:284–307

Chen FK, Li XH, Wang XL, Li QL, Siebel W (2007) Zircon age and Nd–Hf isotopic composition of the Yunnan Tethyan belt, southwestern China. Int J Earth Sci 96:1179–1194

Compston W, Williams IS, Meyer C (1984) U–Pb geochronology of zircons form lunar Breccia 73217 using a sensitive high mass-resolution ion microprobe. J Geophys Res B89:525–534

Cong BL, Wu GY, Zhang Q, Zhang RY, Zhai MG, Zhao DS, Zhang WH (1993) Petrotectonic evolution of the Tethys zone in western Yunnan, China. Chin Bull (B) 23:1201–1207 **(in Chinese)**

Davidson JP (1987) Crustal contamination versus subduction zone enrichment: examples from the Lesser Antilles and implications for mantle source compositions of island arc volcanic rocks. Geochim Cosmochim Acta 51:2185–2198

DeCelles PG, Gehrels GE, Quade J, Ojha TP, Kapp PA, Upreti BN (1998) Neogene foreland basin deposits, erosional unroofing, and the kinematic history of the Himalayan fold-thrust belt, western Nepal. Geol Soc Am Bull 110:2–21

DeCelles PG, Gehrels GE, Quade J, LaReau B, Spurlin M (2000) Tectonic implications of U–Pb zircon ages of the Himalayan orogenic belt in Nepal. Science 288:497–499

DeCelles PG, Gehrels GE, Najman Y, Martin AJ, Carter A, Garzanti E (2004) Detrital geochronology and geochemistry of Cretaceous-Early Miocene strata of Nepal: implications for timing and diachroneity of initial Himalayan orogenesis. Earth Planet Sci Lett 227:313–330

Defant MJ, Drummond MS (1990) Derivation of some modern arc magmas by melting of young subducted lithosphere. Nature 347:662–665

Dewey JF, Shackleton RM, Chang CF, Sun YY (1988) The tectonic evolution of the Tibetan Plateau. Philos Trans R Soc Lond Ser A Math Phys Sci 327:379–413

Dong X, Zhang ZM, Wang JL, Zhao GC, Liu F, Wang W, Yu F (2009) Provenance and formation age of the Nyingchi Group in the southern Lhasa terrane, Tibetan Plateau: petrology and zircon U–Pb geochronology. Acta Petrologica Sinica 25:1678–1694 **(in Chinese with English abstract)**

Dong X, Zhang ZM, Santosh M (2010) Zircon U-Pb Chronology of the Nyingtri Group, Southern Lhasa Terrane, Tibetan Plateau: implications for Grenvillian and Pan-African Provenance and Mesozoic-Cenozoic Metamorphism. J Geol 118:677–690

Evans OC, Hanson GN (1997) Late- to Post-kinematic Archean granitoids of the S.W. Superior Province: derivation through Direct Mantle Melting. Greenstone Belts. Oxford University Press, Oxford, pp 280–295

Fan CJ, Zhang YF (1994) The structure and tectonics of western Yunnan. J SE Asian Earth Sci 9:355–361

Fang ZJ, Zhou ZC, Lin MJ (1990) Some new observations on the geology of western Yunnan. Chin Sci Bull 15:1286–1290

Feng QL (2002) Stratigraphy of volcanic rocks in the Changning-Menglian belt in southwestern Yunnan, China. J Asian Earth Sci 20:657–664

Fontaine H (2002) Permian of Southeast Asia: an overview. J Asian Earth Sci 20:567–588

Gallagher K, Hawkesworth CJ (1992) Dehydration melting and the generation of continental flood basalts. Nature 358:57–59

Garzanti E, Casnedi R, Jadoul F (1986) Sedimentary evidence of a Cambro-Ordovician orogenic event in the Northwestern Himalaya. Sed Geol 48:237–265

Gehrels GE, DeCelles PG, Ojha TP, Upreti BN (2006) Geologic and U–Th–Pb geochronologic evidence for early Paleozoic tectonism in the Kathmandu thrust sheet, central Nepal Himalaya. Geol Soc Am Bull 118:185–198

Gehrels G, Kapp P, DeCelles P, Pullen A, Blakey R, Weislogel A, Ding L, Guynn J, Martin A, McQuarrie N, Yin A (2011) Detrital zircon geochronology of pre-Tertiary strata in the Tibetan-Himalayan orogen. Tecoonics. doi:10.1029/2011TC002868

Geng HY, Brandl G, Sun M, Wong J, Kroner A (2014) Zircon ages defining deposition of the Paleoproterozoic Southpansberg Group and further evidence for Eoarchaean crust in South Africa. Precambr Res 249:247–262

Glassley WE (1974) Geochemistry and tectonics of the Crescent volcanic rocks, Olympic Peninsula, Washington. Geol Soc Am Bull 85(5):785–794

Godin L, Parrish RR, Brown RL, Hodges KV (2001) Crustal thickening leading to exhumation of the Himalayan metamorphic core of central Nepal: insight from U–Pb geochronology and $^{40}Ar/^{39}Ar$ thermochronology. Tectonics 20:729–747

Gong SL, Chen NS, Geng HY, Sun M, Zhang L, Wang QY (2014) Zircon Hf isotopes and geochemistry of the Early Paleoproterozoic high-Sr low-Y quartz-diorite in the Quanji Massif, NW China: crustal growth and tectonic implications. J Earth Sci 25(1):74–86

Halla J (2005) Late Archean high-Mg granitoids (sanukitoids) in the southern Karelian domain, eastern Finland: Pb and Nd isotopic constraints on crust–mantle interactions. Lithos 79:161–178

Healy B, Collins WJ, Richards SW (2004) A hybrid origin for Lachlan S-type granites: the Murrumbidgee batholith example. Lithos 79:197–216

Hirose K (1997) Melting experiments on lherzolite KLB-1 under hydrous conditions and generation of high-mg andesitic melts. Geology 25:42–44

Hoang N, Yamamoto T, Itoh J, Flower MFJ (2009) Anomalous intraplate high-Mg andesites in the Choshi area (Chiba, Central Japan) produced during early stages of Japan Sea opening? Lithos 112:545–555

Honarmand M, Omran NR, Neubauer F, Nabatian G, Emami MH, Quadt A, Dong YP, Bernroider M (2015) Geochemistry of Enclaves and Host Granitoids from the Kashan Granitoid Complex, Central Iran: implications for Enclave Generation by Interaction of Cogenetic Magmas. J Earth Sci 26(5):626–645

Hoskin PWO, Black LP (2000) Metamorphic zircon formation by solid-state recrystallization of protolith igneous zircon. J Metamorph Geol 18:423–439

Hughes NC (2002) Late Middle Cambrian trace fossils from the Lejopyge armata horizon, Zanskar Valley, India, and the use of Precambrian/Cambrian isochronostratigraphy in the Indian subcontinent. Spec Pap Palaeontol 67:135–151

Hutchison CS (1989) Geological evolution of South-east Asia. Clarendon Press, Oxford, pp 1–368

Imayama T, Arita K (2008) Nd isotopic data reveal the material and tectonic nature of the Main Central Thrust zone in Nepal Himalaya. Tectonophysics 451:265–281

Ji WH, Chen SJ, Zhao ZM, Li RS, He SP, Wang C (2009) Discovery of the Cambrianvolcanic rocks in the Xainza area, Gangdese orogenic belt, Tibet, China and its significance. Geol Bull China 9:1350–1354 **(in Chinese with English abstract)**

Kamei A (2004) An adakitic pluton on Kyushu Island, southwest Japan arc. J Asian Earth Sci. doi:10.1016/j.jseaes.2003.07.001

Kamei A, Owaba M, Nagao T, Shiraki K (2004) High-Mg diorites derived from sanukitic HMA magmas, Kyushu Island, southwest Japan arc: evidence from clinopyroxene and whole rock compositions. Lithos 75:359–371

Kawabata H, Shuto K (2005) Magma mixing recorded in intermediate rocks associated with high-Mg andesites from the Setouchi volcanic belt, Japan: implications for Archean TTG formation. J Volcanol Geoth Res 140:241–271

Kelemen PB (1995) Genesis of high-mg andesites and the continental crust. Contrib Miner Petrol 120:1–19

Kelemen PB, Shimuzu N, Dunn T (1993) Relative depletion of niobium in some arc magmas and the continental crust: partitioning of K, Nb, La and Ce during melt-rock reaction in the upper mantle. Earth Planet Sci Lett 120:111–134

Kushiro I (1990) Partial melting of mantle wedge and evolution of island arc crust. J Geophys Res 95:15929–15939

Le Fort P, Tongiorgi M, Gaetani M (1994) Discovery of a crystalline basement and Early Ordovician marine transgression in the Karakorum mountain range, Pakistan. Geology 22:941–944

Li C, Dong YS, Zhai QG, Wang LQ, Yan QR, Wu YW, He TT (2008) Discovery of Eopaleozoic ophiolite in the Qiangtang of Tibet Plateau: evidence from SHRIMP U–Pb dating and its tectonic implications. Acta Petrologica Sinica 24(1):31–36 **(in Chinese with English abstract)**

Li C, Wu YW, Wang M, Yang HT (2010) Significant progress on Pan-African and Early Paleozoic orogenic events in Qinghai-Tibet Plateau: discovery of Pan-African orogenic unconformity and Cambrian system in the Gangdese area, Tibet, China. Geol Bull China 29:1733–1736 **(in Chinese with English Abstract)**

Li ZH, Lin SL, Cong F, Xie T, Zou GF (2012) U–Pb ages of zircon from metamorphic rocks of the Gaoligongshan Group in western Yunnan and its tectonic significance. Acta Petrologica Sinica 28(5):1529–1541 **(in Chinese with English abstract)**

Liang XR, Wei GJ, Li XH, Liu Y (2003) Precise measurement of $^{143}Nd/^{144}Nd$ and Sm/Nd ratios using multiple-collectors inductively coupled plasma-mass spectrometer (MC-ICPMS). Geochimica 32:91–96 (**in Chinese with English abstract**)

Liu BP, Feng QL, Chonglakmani C, Helmcke D (2002) Framework of Paleotethyan Archipelago Ocean of Western Yunnan and its elongation towards North and South. Earth Sci Front 9:161–171 **(in Chinese with English abstract)**

Liu XM, Gao S, Ling WL, Yuan HL, Hu ZC (2006) Identification of 3.5 Ga detrital zircons from Yangtze craton in south China and the implication for Archean crust evolution. Prog Nat Sci 16:663–666

Liu S, Hu RZ, Gao S, Feng CX, Huang ZL, Lai SC, Yuan HL, Liu XM, Coulson IM, Feng GY, Wang T, Qi YQ (2009) U–Pb zircon, geochemical and S–Nd–Hf isotopic constraints on the age and origin of Early Palaeozoic I-type granite from the Tengchong-Baoshan block, western Yunnan Province, SW China. J Asian Earth Sci 36:168–182

Liu YS, Gao S, Hu ZC, Gao CG, Zong KQ, Wang DB (2010) Continental and oceanic crust recycling-induced melt-peridotite interactions in the Trans-north China orogen: U–Pb dating, Hf isotopes and trace elements in zircons from mantle xenoliths. J Petrol 51(1–2):537–571

Ludwig KR (2003) User's manual for Isoplot 3.00: a geochronological toolkit for Microsoft Excel. Geochronology Center Special Publication, Berkeley, pp 1–70

Ma LY, Wang YJ, Fan WM, Geng HY, Cai YF, Zhong H, Liu HC, Xing XW (2014) Petrogenesis of the early Eocene I-type granites in west Yingjiang (SW Yunnan) and its implication for the eastern extension of the Gangdese batholiths. Gondwana Res 25:401–419

McCarron JJ, Smellie JL (1998) Tectonic implications of fore-arc magmatism and generation of high-magnesian andesites: Alexander Island, Antarctica. J Geol Soc Lond 155:269–280

Metcalfe I (1996) Pre-Cretaceous evolution of SE Asian terranes. Tectonic evolution of Southeast Asian. Geol Soc Spl Publ 106:97–122

Metcalfe I (2002) Permian tectonic framework and paleogeography of SE Asia. J Asian Earth Sci 20:551–566

Metcalfe I (2006) Palaeozoic and Mesozoic tectonic evolution and paleogeography of East Asian crustal fragments: the Korean Peninsula in context. Gondwana Res 9:24–46

Metcalfe I (2011) Tectonic framework and Phanerozoic evolution of Sundaland. Gondwana Res 19:3–21

Metcalfe I (2013) Gondwana dispersion and Asian accretion: tectonic and paleogeographic evolution of eastern Tethys. J Asian Earth Sci 66:1–33

Middlemost EAK (1994) Naming materials in the magma/igneous rock system. Earth-Sci Rev 37(3–4):215–224

Miller C, Thöni M, Frank W, Grasemann B, Klötzli U, Guntli P, Draganits E (2001) The early Paleozoic magmatic event in the Northwest Himalaya, India: source, tectonic setting and age of emplacement. Geol Mag 138:237–251

Moyen JF, Martin H, Jayananda M, Auvray B (2003) Late Archaean granites: a typology based on the Dharwar Craton (India). Precambrian Res 127:103–123

Murphy JB, Nance RD (1991) Supercontinent model for the contrasting character of Late Proterozoic orogenic belts. Geology 19:469–472

Myrow PW, Snell KE, Hudges NC, Paulsen TS, Heim NA, Parcha SK (2006a) Cambrian depositional history of the Zanskar Valley region of the Indian Himalaya: tectonic implications. J Sediment Res 76:364–381

Myrow PW, Thompson KR, Hughes NC, Paulsen TS, Sell BK, Parcha SK (2006b) Cambrian stratigraphy and depositional history of the northern Indian Himalaya, Spiti Valley, north-central India. Geol Soc Am Bull 118:491–510

Nie XM, Feng QL, Qian X, Wang YJ (2014) Magmatic record of Prototethyan evolution in SW Yunnan, China: geochemical, zircon U–Pb geochronological and Lu–Hf isotopic evidence from the Huimin metavolcanic rocks in the southern Lancangjiang zone. Gondwana Res 28:757–768

Oliveira MA, Agnol RD, Althoff FJ, da Silva Leite AA (2009) Mesoarchean sanukitoid rocks of the Rio Maria Granite-Greenstone Terrane, Amazonian craton, Brazil. J S Am Earth Sci 27:146–160

Pan GT, Wang LQ, Li RS, Yuan SH, Ji WH, Yin FG, Zhang WP, Wang BD (2012) Tectonic evolution of the Qinghai-Tibet Plateau. J Asian Earth Sci 53:3–14

Parrish RR, Hodges KV (1996) Isotopic constrains on the age and provenance of the Lesser and Greater Himalayan sequences, Nepalese Himalaya. Geol Soc Am Bull 108:904–911

Peate DW, Pearce JA, Hawkesworth CJ, Colley H, Edwards CMH, Hirose K (1997) Geochemical variations in Vanuatu arc lavas: the role of subducted material and a variable mantle wedge composition. J Petrol 38:1331–1358

Prouteau G, Scaillet B, Pichavant M, Maury RC (2001) Evidence for mantle meta-somatism by hydrous silicic melts derived from subducted oceanic crust. Nature 410:197–200 **(Publication 19)**

Qi XX, Li HQ, Li TF, Cai ZH, Yu CL (2010) Zircon SHRIMP U-Pb dating for garnet-rich granite veins in high-pressure granulites from the Namche Barwa complex, eastern syntaxis of the Himalayas, and the relationship with exhumation. Acta Petrologica Sinica 26:975–984 **(in Chinese with English abstract)**

Rapp RP, Watson EB, Miller CF (1991) Partial melting of amphibole, eclogite and the origin of Archaean trondhjemites and tonalites. Precambrian Res 51:1–25

Rapp RP, Shimizu N, Norman MD (1999) Reaction between slab-derived melts and peridotite in the mantle wedge: experimental constraints at 3.8 GPa. Chem Geol 160:335–356

Robinson DM, DeCelles PG, Patchett PJ, Garzione CN (2001) The kinematic evolution of the Nepalese Himalaya interpreted from Nd isotopes. Earth Planet Sci Lett 192:507–521

Rolland Y, Picard C, Pecher A, Lapierre H, Bosch D, Keller F (2002) The cretaceous Ladakh arc of NW Himalaya-slab melting and melt–mantle interaction during fast northward drift of Indian Plate. Chem Geol 182:139–178

Sajona FG, Maury RC, Pubellier M, Leterrier J, Bellon H, Cotton J (2000) Magmatic source enrichment by slab-derived melts in a young post-collision setting, central Mindanao (Philippines). Lithos 54:173–206

Sen C, Dunn T (1994) Dehydration melting of a basaltic composition amphibo-lite at 1.5 and 2.0 GPa: implications for the origin of adakites. Contrib Miner Petrol 117:394–409

Shen SY, Feng QL, Wei QR, Zhang ZB (2008) Newly developed evidence for the original Tethysan island-arc volcanic rocks in the southern segment of the south Lancangjiang belt. Chin J Geochem 26:91–97

Shi C, Li RS, He SP, Wang C, Pan SJ, Liu Y, Gu PY (2010) LA-ICP-MS zircon U–Pb dating for gneissic garnet-bearing biotite granodiorite in Yadong area, southern Tibet, China and its geological significance. Geol Bull China 29:1745–1753 **(in Chinese with English abstract)**

Shimoda G, Tatsumi Y, Nohda S, Ishizaka K, Jahn BM (1998) Setouchi high-Mg andesite revisited; geochemical evidence for melting of subducting sediments. Earth Planet Sci Lett 160:479–492

Shirey SB, Hanson GN (1984) Mantle-derived Archean monozodiorites and trachyandesites. Nature 310:222–224

Shirey SB, Hanson GN (1986) Mantle heterogeneity and crustal recycling in Archean granite–greenstone belts: evidence from Nd isotopes and trace elements in the Rainy Lake province, Ontario, Canada. Geochim Cosmochim Acta 50:2631–2651

Smithies RH, Champion DC (2000) The Archean high-mg diorite suite: links to tonalite–trondhjemite–granodiorite magmatism and implications for early Archean crustal growth. J Petrol 41:1653–1671

Smithies RH, Champion DC, Cassidy KF (2003) Formation of Earth's early Archean continental crust. Precambrian Res 127(1–3):89–101

Smithies RH, Van Kranendonk MJ, Champion DC (2007) The Mesoarchean emergence of modern-style subduction. Gondwana Res 11:50–68

Song SG, Ji JQ, Wei CJ, Su L, Zheng YD, Song B, Zhang LF (2007) Early Paleozoic granite in Nujiang River of northwest Yunnan in southwestern China and its tectonic implications. Chin Sci Bull 52:2402–2406

Stern RA, Hanson GN, Shirey SB (1989) Petrogenesis of mantle derived, LILE-enriched Archean monzodiorites and trachyandesites (sanukitoids) in Southwestern Superior Province, Canada. J Earth Sci 26:1688–1712

Sun SS, McDonough WF (1989) Chemical and isotopic systematics of oceanic basalts: implications for mantle composition and processes. In: Saunders AD, Norry MJ (eds) Magmatism in the Ocean Basins, Special Publications, 42. The Geological Society, London, pp 313–345

Tatsumi Y (2001) Geochemical modeling of partial melting of subducting sediments and subsequent melt–mantle interaction; generation of high-Mg andesites in the Setouchi volcanic belt, Southwest Japan. Geology 29:323–326

Tatsumi Y (2006) High-Mg andesites in the Setouchi Volcanic Belt, Southwestern Japan: analogy to Archean magmatism and continental crust formation? Annu Rev Earth Planet Sci 34:467–499

Tatsumi Y (2008) Making continental crust: the sanukitoid connection. Chin Sci Bull 53(11):1620–1633

Valdiya KS (1995) Proterozoic sedimentation and Pan-African geodynamic development in the Himalaya, the northern frontier of east Gondwanaland. Gondwana Res 1:3–9

Visonà D, Rubatto D, Villa IM (2010) The mafic rocks of Shao La (Kharta, S. Tibet): Ordovician basaltic magmatism in the greater Himalayan crystallines of central-eastern Himalaya. J Asian Earth Sci 38:14–25

Wang YZ (2000) Tectonics and Mineralization of Southern Sanjiang Area. Geology Press, Beijing, pp 45–49 **(in Chinese with English abstract)**

Wang YJ, Fan WM, Zhang HF, Peng TP (2006) Early Cretaceous gabbroic rocks from the Taihang Mountains: implications for a paleosubduction-related lithospheric mantle beneath the central North China Craton. Lithos 86:281–302

Wang YJ, Fan WM, Sun M, Liang XQ, Zhang YH, Peng TP (2007) Geochronological, geochemical and geothermal constraints on petrogenesis of the Indosinian peraluminous granites in the South China Block: a case study in the Hunan Province. Lithos 96:475–502

Wang XL, Zhou JC, Qiu JS, Jiang SY, Shi YR (2008) Geochronology and geochemistry of Neoproterozoic mafic rocks from western Hunan, South China: implications for petrogenesis and post-orogenic extension. Geol Mag 145:215–233

Wang YJ, Zhang YZ, Zhao GC, Fan WM, Xia XP, Zhang FF, Zhang AM (2009) Zircon U-Pb geochronological and geochemical constraints on the petrogenesis of the Taishan sanukitoids (Shandong): implications for Neoarchean subduction in the Eastern Block, North China Craton. Precambrian Res 174:273–286

Wang YJ, Zhang FF, Fan WM, Zhang GW, Chen SY, Cawood PA, Zhang AM (2010) Tectonic setting of the South China Block in the early Paleozoic: resolving intracontinental and ocean closure models from detrital zircon U–Pb geochronology. Tectonics. doi:10.1029/2010TC002750

Wang XX, Zhang JJ, Yang XY, Zhang B (2011) Zircon SHRIMP U–Pb ages, Hf isotopic features and their geological significance of the Greater Himalaya Crystalline Complex augen gneiss in Gyirong area, south Tibet. Earth Sci Front 18:127–139 **(in Chinese with English abstract)**

Wang XX, Zhang JJ, Santosh M, Liu J, Yan SY, Guo L (2012) Andean-type orogeny in the Himalayas of south Tibet: implications for early Paleozoic tectonics along the Indian margin of Gondwana. Lithos 154:248–262

Wang BD, Wang LQ, Pan GT, Yin FG, Wang DB, Tang Y (2013a) U–Pb zircon dating of early Paleozoic gabbro from the Nantinghe ophiolite in the Changning-Menglian suture zone and its geological implication. Chin Sci Bull 58:920–930

Wang YJ, Xing XW, Cawood PA, Lai SC, Xia XP, Fan WM, Liu HC, Zhang FF (2013b) Petrogenesis of early Paleozoic peraluminous granite in the Sibumasu Block of SW Yunnan and diachronous accretionary orogenesis along the northern margin of Gondwana. Lithos 182–183:67–85

Wei GY, Feng GR, Luo ZW, Wu SZ, Tao YY (1984) Stratigraphic sequences of the Lancang and Chongshan Groups in western Yunnan and their volcanism and metamorphism. J Chengdu Coll Geol 2:12–20 **(in Chinese with English abstract)**

Wei GJ, Liang XR, Li XH, Liu Y (2002) Precise measurement of Sr isotopic composition of liquid and solid base using (LP) MC-ICPMS. Geochimica 31:295–299

Williams IS (1998) U-Th–Pb geochronology by ion microprobe. In: McKibben MA, Shanks WC, Ridley WI (eds) Applications of microanalytical techniques to understanding mineralizing processes. Society of Economic Geologists, Colorado, pp 1–35

Williams IS, Claesson S (1987) Isotopic evidence for Precambrian provenance and 854 Caledonian metamorphism of high grade paragneisses from the Seve Nappes, 855 Scandinavian Caledonides. II. Ion microprobe zircon U–Th–Pb. Contrib Miner Petrol 97:205–217

Winchester JA, Floyd PA (1977) Geochemical discrimination of different magma series and their differentiation products using immobile elements. Chem Geol 20:325–343

Wood DA (1980) The application of a Th–Hf–Ta diagram to problems of tectonomagmatic classification and to establishing the nature of crustal contamination of basaltic lavas of the British Tertiary volcanic province. Earth Planet Sci Lett 50(1):11–30

Wu YB, Zheng YF (2004) Gensis of zircon and its constrains on the interpretation of U–Pb age. Chin Sci Bull 49(15):1554–1569 **(in Chinese with English abstract)**

Wu SZ, Tao YY, Feng GR, Wei GY, Luo ZW (1984) Characteristics of metamorphic volcanic rocks in the Lancang and Chongshan Groups. Yunnan Geol 3(2):113–123 **(in Chinese)**

Wu RX, Zheng YF, Wu YB, Zhao ZF, Zhang SB, Liu XM, Wu FY (2006) Reworking of juvenile crust: element and isotope evidence from Neoproterozoic granodiorite in South China. Precambrian Res 146:179–212

Xing XW, Zhang YZ, Wang YJ, Liu HC (2015) Zircon U–Pb geochronology and Hf isotopic composition of the Ordovician granitic gneisses in Ximeng area, west Yunnan Province. Geotectonica et Metallogenia 39(3):470–480 **(in Chinese with English abstract)**

Xu ZQ, Yang JS, Liang FH, Qi XX, Liu FL, Zeng LS, Liu DY, Li HB, Wu CL, Shi RD, Chen SY (2005) Pan-African and Early Paleozoic orogenic events in the Himalayan terrane: inference from SHRIMP U–Pb zircon ages. Acta Petrologica Sinica 21:1–12 **(in Chinese with English abstract)**

Xu MJ, Li C, Xu W, Xie CM, Hu PY, Wang M (2014) Petrology, geochemistry and geochronology of Gabbros from the Zhongcang Ophiolitic Mélange, Central Tibet: implications for an Intra-Oceanic Subduction Zone within the Neo-Tethys Ocean. J Earth Sci 25(2):224–240

Yang YQ, Yang JM, Xu DC, Yang JH (2008) Mineralization of Dapingzhang massive sulfide copper-polymetallic deposit in Yunnan. Mineral Depos 2:230–242 **(in Chinese with English abstract)**

Yang XJ, Jia XC, Xiong CL, Bai XZ, Huang BX, Luo G, Yang CB (2012) LA-ICP-MS zircon U–Pb age of metamorphic basic volcanic rock in Gongyanghe Group of southern Gaoligong Mountain, western Yunnan Province, and its geological significance. Geol Bull China 31:264–276 **(in Chinese with English abstract)**

Yi ZY, Huang BC, Chen JS, Chen LW, Wang HL (2011) Paleomagnetism of early Paleogene marine sediments in southern Tibet, China: implications to onset of the India-Asia collision and size of Greater India. Earth Planet Sci Lett 309:153–165

Yin A, Harrison TM (2000) Geologic evolution of the Himalayan-Tibetan orogen. Annu Rev Earth Planet Sci 28:211–280

Yogodzinski GM, Kay RW, Volynets ON, Koloskov AV, Kay SM (1995) Magnesian andesite in the western Aleutian Komandorsky region: implications for slab melting and processes in the mantle wedge. Geol Soc Am Bull 107:505–519

Yunnan BGMR (Yunnan Bureau Geological Mineral Resource) (1990) Regional geology of Yunnan Province. Geological Publishing House, Beijing, pp 1–729 **(in Chinese)**

Yunnan BGMR (Yunnan Bureau Geological Mineral Resource) (1979) Regional geological survey report in the scale of 1:200,000, Menglian. Geological Publishing House, Beijing 1–145 **(in Chinese)**

Yunnan BGMR (Yunnan Bureau Geological Mineral Resource) (1982) Regional geological survey report in the scale of 1:200,000, Tengchong. Geological Publishing House, Beijing, pp 1–728 **(in Chinese)**

Zhai MG, Cong BL, Qiao GS, Zhang RY (1990) Sm-Nd and Rb-Sr geochronology of metamorphic rocks from SW Yunnan orogenic zones, China. Acta Petrologica Sinica 6:1–11 **(in Chinese with English abstract)**

Zhai QG, Wang J, Li C, Su L (2010) SHRIMP U–Pb dating and Hf isotopic analyses of Middle Ordovician meta-cumulate gabbro in central Qiangtang, northern Tibetan Plateau. Sci China (Ser D) 40(5):565–573 **(in Chinese with English abstract)**

Zhang Q, Li DZ, Zhang KW (1985) Preliminary study on Tongchangjie ophiolite melange from Yun County, Yunnan Province. Acta Petrologica Sinica 1:1–14 **(in Chinese with English abstract)**

Zhang ZM, Wang JL, Shen K, Shi C (2008) Paleozoic circus-Gondwana orogens: petrology and geochronology of the Namche Barwa Complex in the eastern Himalayan syntaxis, Tibet. Acta Petrologica Sinica 24:1627–1637 **(in Chinese with English abstract)**

Zhang YZ, Wang YJ, Fan WM, Zhang AM, Ma LY (2012a) Geochronological and geochemical constraints on the metasomatised source for the Neoproterozoic (~825 Ma) high-mg volcanic rocks from the Cangshuipu area (Hunan Province) along the Jiangnan domain and their tectonic implications. Precambrian Res 220–221:139–157

Zhang ZM, Dong X, Santosh M, Liu F, Wang W, Yiu F, He ZY, Shen K (2012b) Petrology and geochronology of the Namche Barwa Complex in the eastern Himalayan syntaxis, Tibet: constrains on the origin and evolution of the north-eastern margin of the Indian craton. Gondwana Res 21:123–137

Zhao CH (1989) The ATK diagram of basic-intermediate volcanic rocks and tectonic environment. Geol Sci Technol Inf 8(4):1–5 **(in Chinese with English abstract)**

Zhong DL (1998) Paleo-Tethyan Orogenic Belt in the Western Parts of the Sichuan and Yunnan Provinces. Science Press, Beijing, pp 1–231 **(in Chinese with English abstract)**

Zhou ZG, Liu WC, Liang DY (2004) Discovery of the Ordovician and its basal conglomerate in the Kangmar area, southern Tibet—with a discussion of the relation of the sedimentary cover and unifying basement in the Himalayas. Geol Bull China 23:655–663 **(in Chinese with English abstract)**

Zhu DC, Zhao ZD, Niu YL, Dilek Y, Mo XX (2011) Lhasa terrane in southern Tibet came from Australia. Geology 39:727–730

Zhu DC, Zhao ZD, Niu YL, Dilek Y, Wang Q, Ji WH, Dong GC, Sui QL, Liu YS, Yuan HL, Mo XX (2012a) Cambrian bimodal volcanism in the Lhasa Terrane, southern Tibet: record of an early Paleozoic Andean-type magmatic arc in the Australian proto-Tethyan margin. Chem Geol 328:290–308

Zhu DC, Zhao ZD, Niu YL, Wang Q, Dilek Y, Dong GC, Mo XX (2012b) Origin and Paleozoic tectonic evolution of the Lhasa Terrane. Geol J China Univ 18:1–15 **(in Chinese with English abstract)**

Zi JW, Cawood PA, Fan WM, Tohver E, Wang YJ, McCuaig TC (2012a) Generation of Early Indosinian enriched mantle-derived granitoid pluton in the Sanjiang Orogen (SW China) in response to closure of the Paleo-Tethys. Lithos 140–141:166–182

Zi JW, Cawood PA, Fan WM, Wang YJ, Tohver E, McCuaig TC, Peng TP (2012b) Triassic collision in the Paleo-Tethys Ocean constrained by volcanic activity in SW China. Lithos 144–145:145–160